Titania and Alumina Supported Co-Mo Catalysts for Hydrogenation of Sulfur Compounds: A Morphology and Reactivity Study

Christopher B. Lavery, Ruohong Sui, John H. Jacobs, Connor E. Deering,
Dao Li, and Robert A. Marriott

Presented at the Brimstone Sulfur Symposium, September 2023

ABSTRACT

Metal oxide-supported Co-Mo sulfides have played an important role in increasing sulfur recovery efficiencies through the hydrogenation of sulfur-containing species within a Claus tail gas. In this study, the hydrogenation activity of a TiO_2-supported Co-Mo catalyst was compared to that of a more traditional Al_2O_3-supported Co-Mo material under various process conditions. The observed differences in activity were attributed to the pore structure within the anatase TiO_2 support. Indeed, the TiO_2 pore structure promoted formation of smaller 2H MoS_2 nanocrystals that were better dispersed with more accessible active sites. All catalysts used in this study were non-commercial and prepared in-house.

The main elements of this investigation were:

i) In addition to testing a generic protocol for sulfiding and reducing the supported Co-Mo catalysts that utilizes a specific N_2-, H_2-, and H_2S-containing feed, we explored the use of a representative Claus tail gas itself as the sulfiding and reducing environment. Collectively, our results indicate the TiO_2-supported material led to more efficient reduction of MoS_3 to the active MoS_2, compared to the Al_2O_3-supported counterpart. While sulfiding Co-Mo catalysts with a tail gas may afford equilibrium activity in some instances, the conventional sulfiding procedure led to a more active catalyst.

ii) The effect of H_2 exposure in the absence of H_2S on tail gas catalyst activity was also investigated. This scenario may happen when a commercial sulfur recovery unit goes into hot standby mode. Our results show that this exposure can be detrimental to the catalyst if it occurs while in the oxide form; however, the sulfided catalysts were found to be more robust towards activity loss.

iii) Finally, the impact of oxygen ingress on the sulfided form of both the Al_2O_3- and TiO_2-supported materials was investigated. Both catalysts suffered some loss in activity after exposure to the oxygen ingress conditions. When the oxygen ingress occurred at 280 °C, the Al_2O_3-supported material was more sensitive to oxygen ingress. However, when the oxygen ingress was simulated at 400 °C, the losses in activity were more comparable between the two materials. Interestingly, compared to the 280 °C exposure test, the O_2

ingress at 400 °C was less damaging to the Al_2O_3-supported material but more detrimental to the TiO_2-supported catalyst.

1. Introduction

The demand for (i) low-carbon natural gas, (ii) phosphate based fertilizers (using sulfuric acid), (iii) sulfuric acid based metal extraction and (iv) lower sulfur fuels are expected to increase for years to come. In addition to increasing demand though, population growth and metal intensive technologies, such as electric vehicles,and environmental concerns provides incentive for industry to lower sulfur emissions further. As such, energy companies are continuously improving operational efficiencies and sulfur removal technologies. To separate hydrogen sulfide (H_2S) and carbon dioxide (CO_2) from methane (CH_4), an amine scrubbing unit has been widely used followed by a sulfur recovery unit, where the modified Claus process is used to convert the separated H_2S to elemental sulfur (S_8) which is then primarily used for producing sulfuric acid and fertilizers [1-3]. The same sulfur recovery technology is used after sulfur removal within refining. With three catalyst in-line beds, the sulfur recovery from H_2S within the thermal and catalytic stages of the modified Claus process is equilibrium limited at *ca.* 98%. As such, there is still *ca*. 1% H_2S, 0.5 % SO_2, and hundreds to thousands parts per million by volume (ppmv) of COS and CS_2 in a typical Claus tail gas [4, 5]. These residual sulfur compounds are often treated by use of a tail gas treatment unit, where SO_2, COS, CS_2, and S_8 vapour are hydrogenated to H_2S which is then captured by low-pressure H_2S-selective amine and recycled back into the modified Claus process to achieve a sulfur recovery of >99.9% [6]. The off-gas from the tail gas amine, containing very small levels of sulfur species, is then sent to a final thermal oxidizer unit before it is emitted to the atmosphere.

Molybdenum and tungsten sulfides promoted by cobalt or nickel have been extensively studied to catalyse sulfur hydrogenation reactions [7]. These types of transition-metal-sulfide catalysts have a long history of being used for desulfurizing coal oils, crude oils and ammonia synthesis. Molydenum with cobalt sulfides are used in hydrogenating sulfur species in Claus tail gases and crude oils. The catalytic mechanism for organo-sulfur species has been discussed since the development of these materials in 1928 [8]. Today, the so-called Co–Mo–S model is generally accepted [6, 9-11]. In this model, the active sites are located on the edge of 2D MoS_2, where the coordination sphere of Mo is unsaturated with sulfur (Scheme 1, active site). Within this active site, the Mo chemisorbs sulfur compounds (R–S) while the adjacent sulfur atoms split a hydrogen molecule (H_2) into hydrogen atoms and form S–H bonds, (Steps 1 and 2, Scheme 1). After loss of the R group from the chemisorbed sulfur compound (Step 3, Scheme 1), the active site is poised to release H_2S that can then leave the catalyst edges (Step 4, Scheme 1), and, in turn, the active site is regenerated.-

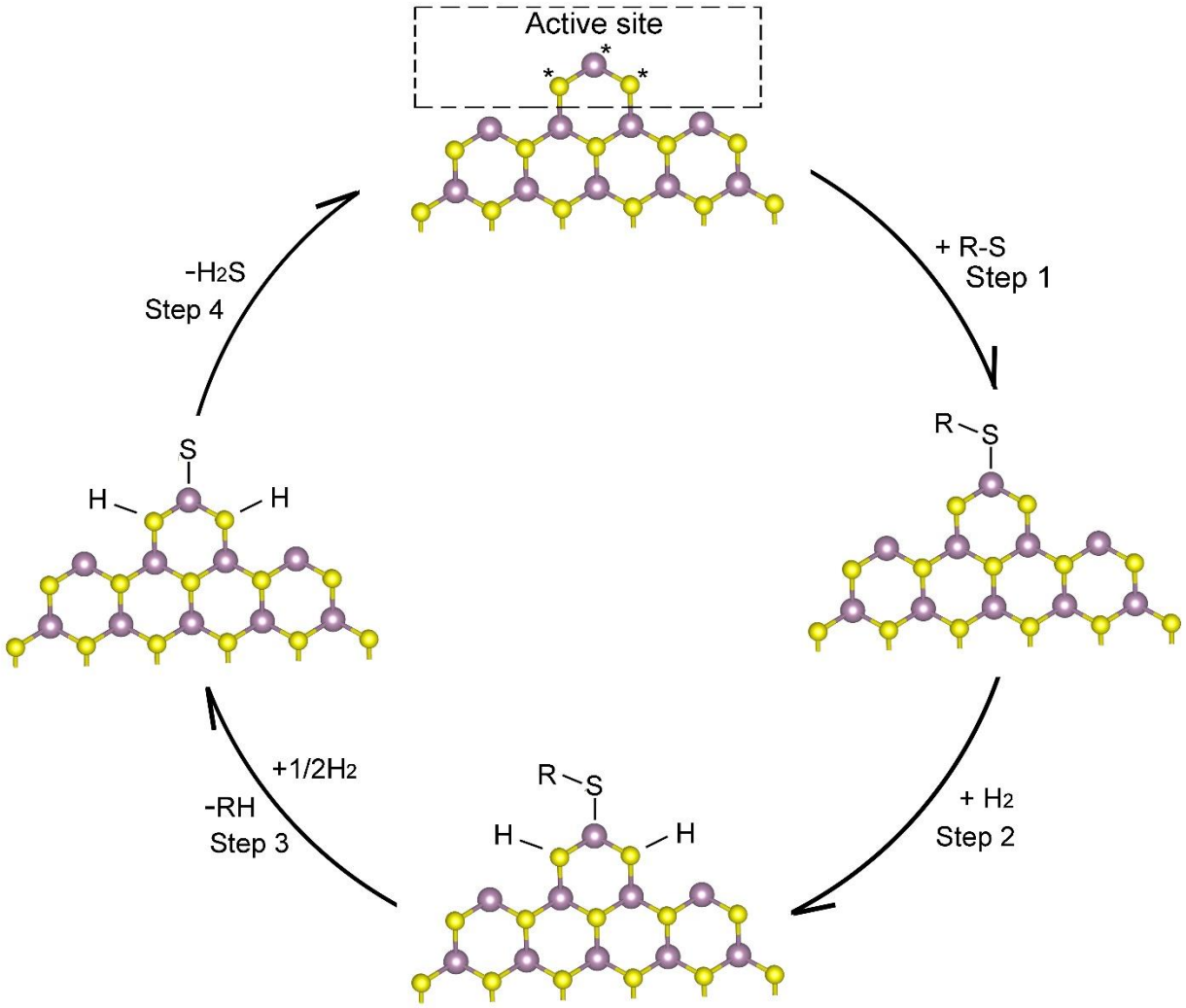

Scheme 1. Simplification of Co–Mo–S model for 2D MoS_2. Yellow balls = S, purple balls = Mo, and (*) indicates Mo and S atoms with an unsaturated coordination sphere within active site. In reality, there are two layers of sulfur atoms: one is above (as shown) and another is under the Mo plane (hidden underneath the top sulfur layer for clarity).

Because the active sites are located on the MoS_2 edges, good dispersion is important for effective catalytic activity with an increased concentration of edges. To maintain this dispersion cobalt is added to the catalyst. Note that this mechanism is thought to be the same for both organo-sulfur hydrogenation catalysts and hydrogenation of sulfur species in a Claus Tail Gas. Because edges must be accessible by process fluids, supported Co-Mo catalysts prepared by impregnation are more attractive than those prepared by the bulk format [6]. Due to its reasonable cost and thermal/mechanical stability, Al_2O_3 has been widely used as a Co-Mo support for industrial hydrogenation processes. Additionally, the hydroxyl bonds (–OH) of Al_2O_3 have been found to interact with MoO_3, the precursor of MoS_2, which is favourable for promoting good dispersion during the impregnation method [12]. There is also literature precedent for using TiO_2 as a Co-Mo

catalyst support in some hydrogenation applications. It was found that the TiO_2 supported materials were more active for the hydrodesulfurization of organosulfur compounds (thiophene and dibenzothiophene) compared to the analogous Al_2O_3 supported material [13-15]. We note that Al_2O_3 still has certain advantages over TiO_2 when considering cost, thermal stability, and mechanical strength [16].

In addition to the electronic properties, the pore structure of the catalyst support also plays a key role in the resulting activity for two reasons: (i) the need to accommodate the deposited species [17], and (ii) the need to accommodate the diffusion of reactant molecules within the support pellets so they can reach catalyst active sites. Therefore, the porosity and pore size distribution of the catalyst support, along with the morphology of the deposited species, is considered when a catalyst is designed. Note that pore size or diameter (d) distribution is equally if not more important than total surface area. In this context, the catalyst support may have micropores (d <2 nm), mesopores (2> d <50 nm), and/or macropores (d >50 nm). Co-Mo catalyst supports must be able to accommodate two-dimensional (2D) MoS_2 crystallites which have been observed in the 4-10 nm range [11, 18, 19].

Catalyst manufactures offer pre-sulfided Co-Mo tail gas hydrogenation catalysts that require care during transportation and loading to prevent conversion back to the original oxide form. However, it is also common for the oxide form of the Co-Mo catalyst to be supplied, which then needs to be converted into the active sulfide within the hydrogenation reactor. This involves both the conversion of MoO_3 to MoS_3 and reduction of MoS_3 to MoS_2 [20]. A representative *in-situ* procedure would involve flowing 2.5 mol% H_2S and 10 mol% H_2 (balanced with N_2) while applying a slow temperature ramp from *ca.* 200 to 320 °C and controlling the exotherm across the catalyst bed to δT < 50 °C. Previous research has shown that a temperature soak at the high end of the temperature ramp is also important for the conversion of MoS_3 to MoS_2, and assembly of amorphous MoS_2 into crystalline slabs [21]. Due to the need for separate feeds of H_2S and H_2, which are not always easily accessible, and temperature limitations in some cases (*i.e.*, indirect steam reheaters), it is of inteterest to explore alternative sulfidation protocols and examine the resulting impact on catalyst activity. One such scenario that was investigated in this study involved the use of a Claus tail gas itself as the sulfiding and reducing environment.

There has also been some questions within the sulfur industry on how exposure to different process conditions can influence the Co-Mo hydrogenation catalyst's health. The two scenarios investigated in the current study included: i) exposure to hydrogen in the absence of H_2S at elevated temperatures [22], before and after catalyst sulfiding, and ii) O_2 ingress from a faulty direct-fired reheater. In this context, the purpose of this research was to investigate the efficacy of an alternative sulfiding protocol, in addition to studying the effect of H_2 exposure and O_2 ingress on Co-Mo catalyst activity. Both alumina- and titania-supported materials were investigated [23].

For commercial sensitivity reasons, both the alumina- and titania-supported Co-Mo catalysts were prepared in-house to perform the above investigations. To relate catalyst morphology and the observed reactivity, the materials were studied by N_2 physisorption, thermogravimetric analysis (TGA), powder X-ray diffraction (PXRD), X-ray photoelectron spectroscopy (XPS), and high-resolution transmission electron microscopy (HRTEM) equipped with selected area electron diffraction (SAED). The catalyst tests were carried out in an isothermal fix-bed continuous-flow reactor, and the catalytic performance was monitored using gas chromatography (GC) analysis.

2. Methods

2.1. Materials

98.0% $(NH_4)_6Mo_7O_{24}{\cdot}4H_2O$ (82.6% MoO_3, Fisher), 98.0% $Co(NO_3)_2{\cdot}6H_2O$ (Thermo Scientific), γ-Al_2O_3 (1.6 mm extrudate, Saint-Gobain), 67.5% $TiOSO_4$ (with 8.9% H_2SO_4 and 23.6 H_2O, Alfa Aesar), 97% $Ti(O^iPr)_4$ and 99% CS_2 (Sigma−Aldrich) were used without further purification. CO_2, N_2, and helium were purchased from Praxair (Canada) with a purity of 99.999%. H_2S and SO_2 were also purchased from Praxair (Canada) but had purities of 99.6% and 99.98%, respectively.

2.2. Preparation of the catalyst supports

The γ-Al_2O_3 support was prepared by resizing the 1.6 mm *d* extrudates into *ca.* 3 mm long rods. The anatase TiO_2 support was prepared from titanyl sulfate ($TiOSO_4$), a feedstock of commercial TiO_2 [24], by using a sol–gel method as reported earlier [25]. The as-prepared TiO_2 was crushed into particles ($d < 2$ mm) before the addition of deionized water to make a paste. The paste was compressed into a cake by using a stainless-steel tubular column (i.d. = 38.1 mm and length = 152 mm) and a piston at 3000 psi. The cake was dried at 80 °C under a vacuum (2.7 kPa) for 8 hrs before calcination in air at 400 °C for 2 hrs and then cutting and sieving. The resulting granules with a *d* of *ca.*1.5 mm were used for TiO_2 support.

2.3. Preparation of the catalysts: Impregnation of Co-Mo on the catalyst support

In a typical synthesis, 7.47 g of $(NH_4)_6Mo_7O_{24}{\cdot}4H_2O$ (corresponding to 16.2 wt% MoO_3 in the final product) was dissolved in 30 g of deionized water (solution A) at room temperature. Separately, 5.52 g of $Co(NO_3)_2{\cdot}6H_2O$ (3.8 wt% CoO in the final product) was dissolved in 10 g of deionized water (solution B). Solution A and B were both transparent (A was colorless and B was dark red) and were added to 40 g of TiO_2 or Al_2O_3 in a 200 mL beaker, one immediately after the other, under constant stirring with a glass rod. With both materials, there was a few mL of excess liquid (pink solution) remaining in the beaker along with the wet catalyst support. The resulting mixture was put in the oven at 50 °C without disturbing for 10 hrs, followed by vacuum at 80 °C for 8 hrs and calcination at 400 °C in air for 2 hrs.

The bulk densities of that CoMo(oxide)/Al_2O_3 catalyst and CoMo(oxide)/TiO_2 catalyst were 700 and 750 $kg{\cdot}m^{-3}$, respectively.

2.4. Experimental setup for catalytic studies

The catalytic studies were performed in a system that is represented by Scheme 2. The toxic gases (orange area) were located in a ventilated storage bay. The feed gases were delivered using mass flow controllers (MFC, Brooks SLA 5800 series) that were controlled by a LabView program. Deionized water was added using a syringe pump (Cole Parmer 74900 Series) and vaporized in a stainless steel coil (393 K) that was swept with the feed N_2. SO_2 and O_2 were fed to the reactor separately from the gas mixture containing H_2S to prevent pre-reactions prior to the entire feed entering the reactor. A pressure gauge, relief valve, and bypass valve were used for safety purposes. The vertical stainless steel reactor (2.1 cm i.d.) was equipped with four thermal couple wells (located at different levels within the catalytic bed) that were interfaced with the Labview program via a TC-08 sensor (Pico Technology). At the bottom of the reactor, there was a stainless steel mesh for supporting the catalyst pellets. The furnace was heated by a fluidized sandbath and the temperatures were set using a Digi-Sense Controller (Cole Parmer). The reactor was isothermal along its entire length to within ±1 °C. The reactor outlet was plumbed to two condensers that were heat traced accordingly for trapping liquid sulfur. The reactor effluent then passed through a dry trap followed by an aqueous KOH trap to collect any unreacted H_2S and SO_2, before being vented to the lab plenum and ultimately to the outside atmosphere. The setup contained two sampling ports at both the inlet (for feed check) and outlet (to determine the product concentrations) of the reactor. The product composition was analyzed using a Varian GC equipped with two columns (Rt® u-Bond for CO_2, H_2S, COS, SO_2, and CS_2 analysis, and RT®-Molseive 5A, Restek, for H_2, N_2, and CO analysis) coupled with two thermal conductivity detectors (TCDs). All gas samples were drawn through P_2O_5 cartridges to capture any condensables (*i.e.,* H_2O and sulfur), and to avoid any reaction on the Rt® u-Bond column.

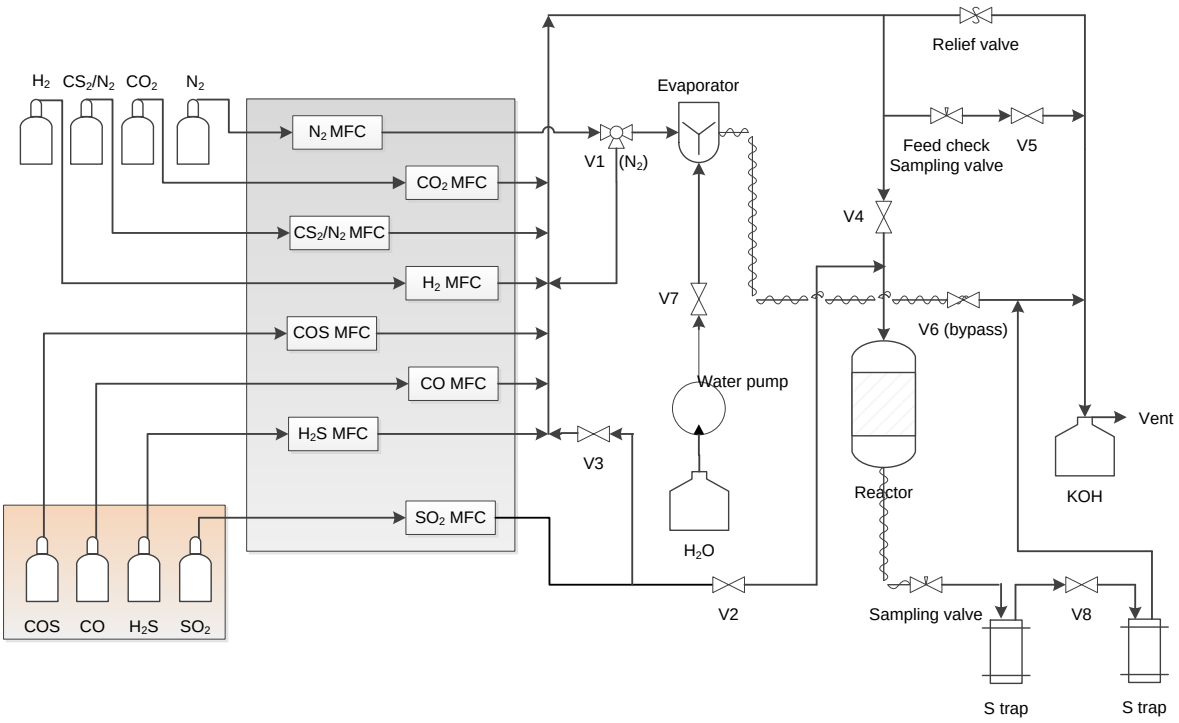

Scheme 2. Experimental setup for catalytic studies.

Safety notes: because this research involved the use of toxic gases H_2S and SO_2, all catalytic tests were conducted in a walk-in bay equipped with high-velocity ventilation, permanent gas detectors, and a caustic scrubbing system. The detectors are interfaced with solenoids controlling air-operated valves to allow (air on) gas flow from a separate and ventilated storage bay. In the case of a leak leading to toxic gas concentrations exceeding 5 ppmv H_2S, 2 ppmv SO_2, or 10 ppmv CO, the air-operated valves close and all toxic gas flow to the experimental system stops.

2.5. Sulfidation of Co-Mo catalysts

The gas streams used for sulfiding the Co-Mo catalysts were: (i) 1.0 or 2.5 mol% H_2S, 10 mol% H_2, bal. N_2 at a gas hourly space velocity(GHSV) of 500 h^{-1} (STP) , and (ii) a representative Claus tail gas containing H_2, H_2S, SO_2, CO_2, H_2, CO, COS, CS_2, H_2O, and N_2 at a GHSV of 1250 h^{-1} (STP) with the concentrations as described below.

(i) 35 mL of CoMo(oxide)/Al_2O_3 or CoMo(oxide)/TiO_2 was loaded into the stainless-steel reactor under 100 mL·min^{-1} of N_2 flow. The reactor was heated from ambient temperature to 200 °C, then the 1.0 or 2.5 mol% H_2S, 10 mol% H_2, and balance N_2 feed was introduced to the catalyst bed and a temperature ramp of 14 °C·hr^{-1} until T = 315 °C was achieved. The feed was maintained for 4 hrs at 315 °C, followed by 100 mL·min^{-1} N_2 purging and adjustment to the desired experimental temperature (220-260 °C) for the catalytic performance tests.

(ii) 35 mL of CoMo(oxide)/Al_2O_3 or CoMo(oxide)/TiO_2 was loaded in the reactor and the catalyst was pretreated with a representative Claus tail gas with a target composition of 1.2 mol% H_2S, 0.4

mol% SO_2, 8.0 mol% CO_2, 1.7 mol% H_2, 0.7 mol% CO, 300 ppmv COS, 300 ppmv CS_2, 30.0 mol% H_2O, and balance N_2 at 533 K at a GHSV of 1250 h^{-1} (STP).

2.6. Catalytic studies

After the sulfidation of each fresh catalyst, the tail gas stream (with the concentrations as described above) was passed through the 35 mL catalyst bed with a total flow rate of 785 $mL \cdot min^{-1}$, corresponding to a GHSV of 1250 h^{-1} (STP).

COS conversion was calculated using the equation below:

$$\%\text{COS Conversion} = 100\frac{[\text{COS}]_i - [\text{COS}]_f\left([\text{N}_2]_f/[\text{N}_2]_i\right)}{[COS]_i} \quad (1)$$

where $[COS]_i$ and $[N_2]_i$ are the mol% of COS and N_2 in the feed, and $[COS]_f$ and $[N_2]_f$ are the mol% of COS and N_2 in the product stream, as measured by GC analysis.

2.7. Catalyst Characterizations

The used catalysts were stored in a glovebox under a helium environment, and caution was taken to minimize exposure to air before each analysis. N_2 physisorption measurements were conducted using a 3Flex (Micromeritics) instrument. Before each adsorption measurement, the samples were degassed in situ at 200 °C until a vacuum of 1.33×10^{-7} bar was reached. PXRD was performed using a Rigaku Ultima IV diffractometer at a speed of 2° min^{-1} and a step size of 0.02°. XPS was collected on a Kratos AXIS Supra Spectrometer that probes the surface of the sample to a depth of 7-10 nm and has detection limits ranging from 0.1 to 0.5 atom % depending on the element. The survey spectra were obtained from an area of approximately 300 × 700 microns using a pass energy of 160 eV, while the high-resolution spectra were obtained from an area of approximately 300 × 700 microns using a pass energy of 20 eV. HRTEM and SAED images were collected using a Tecnai 20 operated at 200 kV. The TGA measurements were performed on a SETARAM LABSYS EVO TGA system that was connected to three mass flow controllers for delivering He, N_2, and H_2S. The catalyst mass was determined by measuring the dry sample after the subtraction of the weight of the crucible with support, and the latter was measured under a blank condition (flowing the feed gas mixture without a sample).

2.8 Abbreviations

BET: Brunauer-Emmett-Teller
FFT: fast Fourier transform
HAc: acetic acid
HRTEM: high-resolution transmission electron microscopy
IC: Ionic chromatography
PXRD: powder X-ray diffraction
SAED: selected area electron diffraction

TGA: thermogravimetric analysis
XPS: X-ray photoelectron spectroscopy
XRD: X-ray diffraction

3. Results and discussion

3.1. Sulfidation Studies

3.1.1. Effect of H_2S Concentration during Sulfiding by Conventional Method

After loading the fresh Co-Mo catalyst in the fixed-bed reactor, the sulfidation process was monitored by measuring the H_2S concentrations in the reactor effluent. From Figure 1a, for the CoMo(oxide)/Al_2O_3 catalyst, we can see it took *ca.* 12 hrs for the effluent H_2S to reach the inlet concentration when 1.0 mol% H_2S was used but only *ca.* 5 hrs when 2.5 mol% H_2S was used. Evidently, the higher concentration minimized any H_2S starvation within the bed early on in the sulfiding process, and allowed for the 4-hr temperature soak to occur with a fully sulfided bed. The effluent H_2S that was measured during sulfiding of the CoMo(oxide)/TiO_2 material is shown in Figure 1b. Interestingly, there was excess H_2S measured (*i.e.*, the outlet H_2S concentration was greater than the inlet H_2S concentration) under the 1.0 mol% H_2S condition. This H_2S "roll-up effect" was attributed to the hydrogenation of residual sulfate trapped in the bulk titania (Eq. 2) [25, 26].

$$TiOSO_4 + 4H_2 \rightarrow H_2S + TiO_2 + 3H_2O \qquad (2)$$

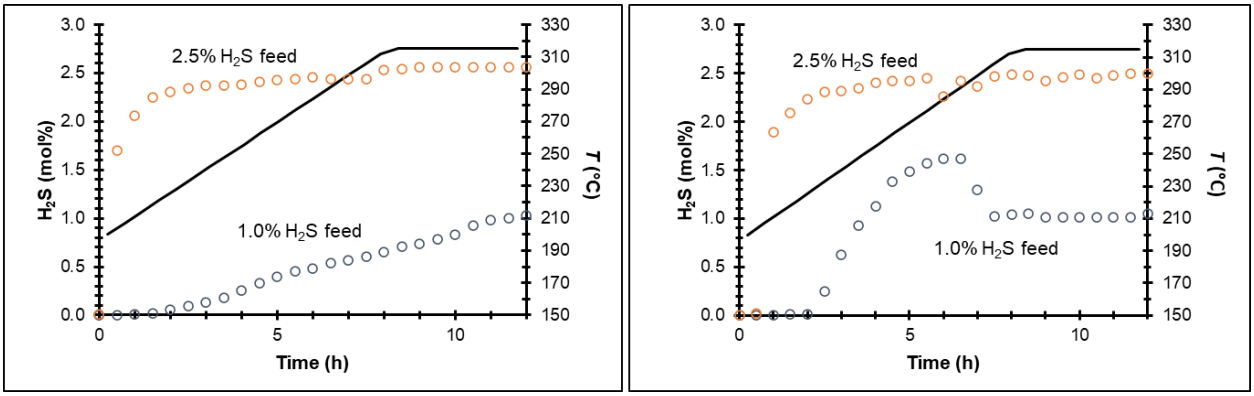

Figure 1. (a) The H_2S breakthrough concentration profiles during sulfiding of CoMo(oxide)/Al_2O_3 and (b) CoMo(oxide)/TiO_2. Notes: orange circles represent effluent H_2S concentrations when the feed contained 2.5 mol% H_2S and 10 mol% H_2 (balanced with N_2), and dark blue circles represent effluent H_2S concentrations when the feed contained 1.0 mol% H_2S and 10 mol% H_2 (balanced with N_2). The black lines correspond to the reactor temperature.

For reasons previously described, one of the first signs of tail gas catalyst deactivation is a loss in COS conversion [23]. Indeed, this parameter offers insight into the extent of the water gas shift reaction which converts CO to CO_2 and active surface bound hydrogen by reaction with water. A loss in water gas shift reaction activity can manifest in increased COS concentrations from the sour

gas shift reaction or by direct combination of CO with sulfur. As a result of this, monitoring COS hydrolysis under Claus tail gas conditions serves as a useful methodology for measuring tail gas catalyst activity that takes into account both the hydrogenation and hydrolysis functions of the catalyst [23]. Based on the COS conversions shown in Figure 2, sulfiding with 2.5 mol% H_2S does manifest better catalytic activity; in particular for the CoMo(sulfide)/Al_2O_3 sample. When 2.5 mol% H_2S was used, the CoMo(sulfide)/Al_2O_3 catalyst only deviated away from equilibrium COS conversion at 220 °C (Figure 2b). When 1.0 mol% H_2S was used, COS conversion fell below equilibrium levels at 240 and 220 °C (Figure 2a). There was no observable diference in the CoMo(sulfide)/TiO_2 catalytic performance whether 1.0 (Figure 2a) or 2.5 mol% (Figure 2b) H_2S was used during sulfiding; in both cases, equilibrium COS conversion was obtained across all experimental temperatures (220-280 °C).

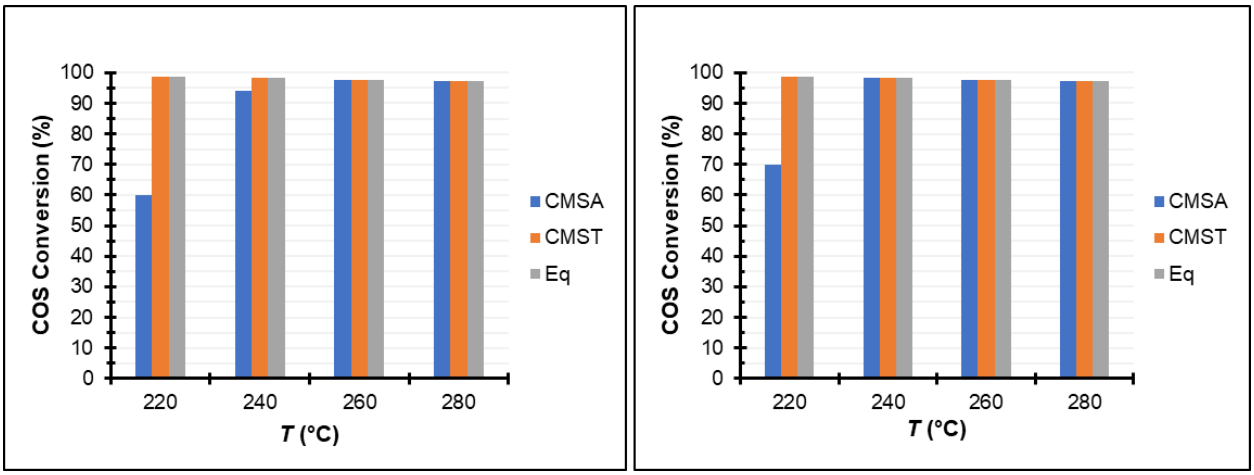

Figure 2. (a) COS conversions offered by CoMo(sulfide)/Al_2O_3 (CMSA) and CoMo(sulfide)/TiO_2 (CMST) after conventional sulfiding with 1.0 mol% H_2S; and (b) COS conversions offered by CoMo(sulfide)/Al_2O_3 (CMSA) and CoMo(sulfide)/TiO_2 (CMST) after conventional sulfiding with 2.5 mol% H_2S. The Claus tail gas feed used during performance testing is described in section 2.5.

3.1.2. TGA Studies during Sulfiding by Conventional Method

While employing the 2.5 mol% H_2S, 10% H_2, and balance N_2 feed, the sulfidation process was also monitored by the catalyst weight change under isothermal conditions at three temperatures: 246, 280, and 323 °C. The weight gain of CoMo(oxide)/Al_2O_3 in Figure 3a was mainly attributed to the conversion of the Co-Mo oxides (O atomic weight = 16.00 g·mol^{-1}) to the corresponding sulfides (S atomic weight = 32.07 g·mol^{-1}) [27]. It was surprising to see that a lower temperature was favorable for the weight gain at the beginning of the sulfidation process (within 1 hr in Figure 3a). It is noted that, while a higher temperature is kinetically favorable for sulfidation, a lower temperature will be thermodynamically favorable for this exothermic reaction (see Eq. 3). Additionally, lower temperatures are more favourable for adsorption of the sulfiding gas species which may also lead to an initial accelerated mass change. The weight loss of CoMo(oxide)/TiO_2 in Figure 3b was mainly assigned to the reduction and removal of sulfate residue from the TiO_2

support (see equation 2), which was synthesized from $TiOSO_4$. The weight gain from sulfiding was not enough to compensate for the weight loss from the removal of sulfate.

$$MoO_3 + H_2 + 2H_2S \rightleftharpoons MoS_2 + 3H_2O,\ \Delta H_{600K} = -229.3\ kJ \qquad (3)$$

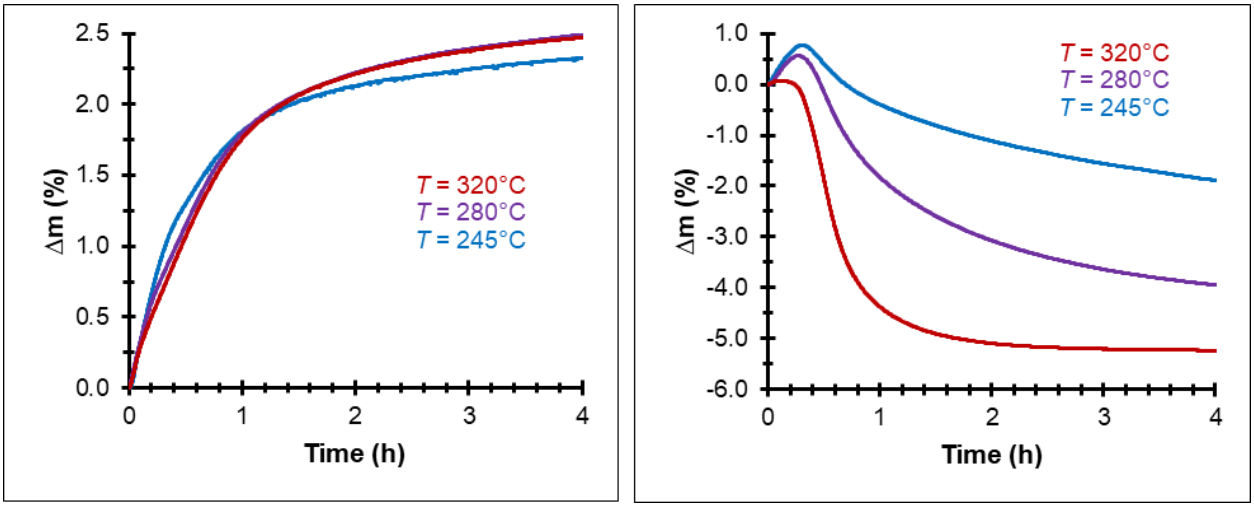

Figure 3. (a) TGA during sulfiding of CoMo(oxide)/Al_2O_3, and (b) TGA during sulfiding of CoMo(oxide)/TiO_2.

The intention of these TGA studies was to compare sulfiding rates of CoMo(oxide)/Al_2O_3 versus CoMo(oxide)/TiO_2 under the same conditions but the presence of sulfate on the CoMo(oxide)/TiO_2 material made this comparison difficult. However, the TGA results do indicate a faster stabilization in mass for the CoMo(oxide)/TiO_2 material at 596 K compared to the CoMo(oxide)/Al_2O_3 catalyst.

3.1.3. Investigation into Sulfiding with a Representative Claus Tail Gas

As described in the introduction, there is motivation for exploring alternative sulfiding procedures. One alternative method that was investigated here involved the use of a representative Claus tail gas as the sulfiding and reducing environment. Fresh CoMo(oxide)/Al_2O_3 or CoMo(oxide)/TiO_2 was loaded in the reactor and exposed to Claus tail gas conditions at 260 °C for 30 hrs in the case of CoMo(oxide)/Al_2O_3, and 10 hrs in the case of CoMo(oxide)/TiO_2 (please see section 2.5 for the tail gas composition). The extent of sulfiding was then investigated by measuring the COS conversion at different temperatures. These results are presented in Figure 4b and, for the sake of comparison, the COS conversions offered after the conventional sulfiding procedure are presented in Figure 4a. After sulfiding with a Claus tail gas, the CoMo(sulfide)/TiO_2 material offered equilibrium COS conversions from 240 to 280 °C but fell *ca.* 40% below equilibrium at 220 °C. The CoMo(sulfide)/Al_2O_3 catalyst only offered equilibrium COS conversion at 280 °C after sulfidation with the Claus tail gas and fell *ca.* 20% below equilibrium at 260 °C. There was no obvious increase in COS conversion for the CoMo(sulfide)/Al_2O_3 catalyst at 260 °C after 30 hrs online.

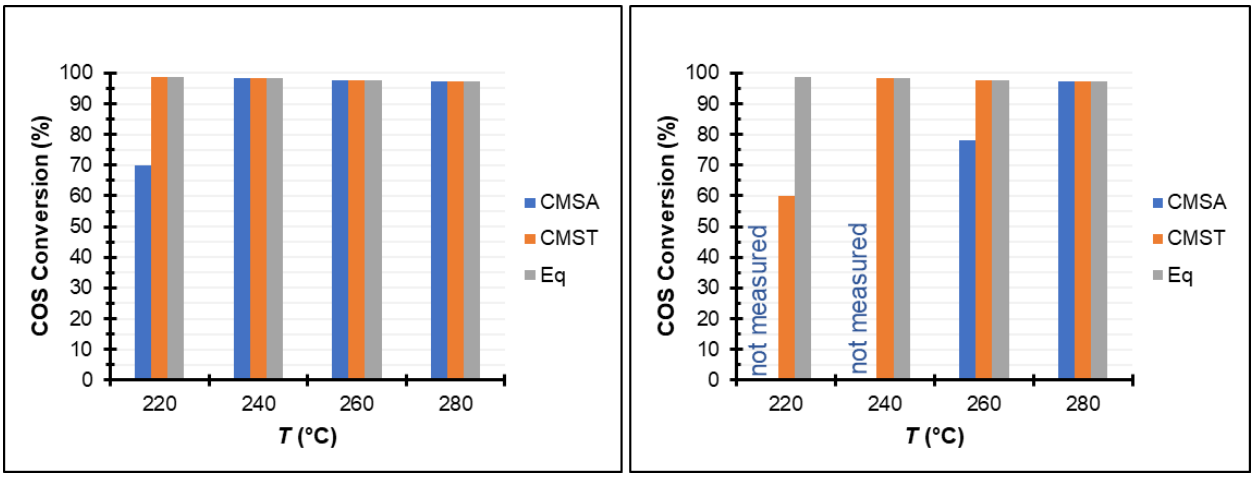

Figure 4. (a) COS conversions offered by CoMo(sulfide)/Al_2O_3 (CMSA) and CoMo(sulfide)/TiO_2 (CMST) after conventional sulfiding with 2.5 mol% H_2S; and (b) COS conversions offered by CoMo(sulfide)/Al_2O_3 (CMSA) and CoMo(sulfide)/TiO_2 (CMST) after sulfiding with a representative Claus tail gas at 260 °C.

3.2. H_2 Exposure in the Absence of H_2S

3.2.1. H_2 Exposure in the Absence of H_2S Prior to Sulfiding

The impact of H_2 exposure in the absence of H_2S, 10% H_2 in balance N_2 at 260 °C for 8 hrs, on the oxide version of the catalysts (CoMo(oxide)/Al_2O_3 or CoMo(oxide)/TiO_2) prior to sulfiding is shown in Figure 5b. For the sake of comparison, the COS conversions offered after the conventional sulfiding procedure, with no H_2 exposure in the absence of H_2S, are presented in Figure 5a. While the COS conversions from 240-280 °C were still at equilibrium levels, both the alumina and titania-supported materials suffered a small loss in conversion at 220 °C (Figure 6b) compared to the baseline performance established after the conventional sulfiding procedure with no H_2 exposure in the absence of H_2S (Figure 5a). These results indicate that care should be taken when sulfiding a catalyst to not expose the oxide form to H_2 in the absence of H_2S.

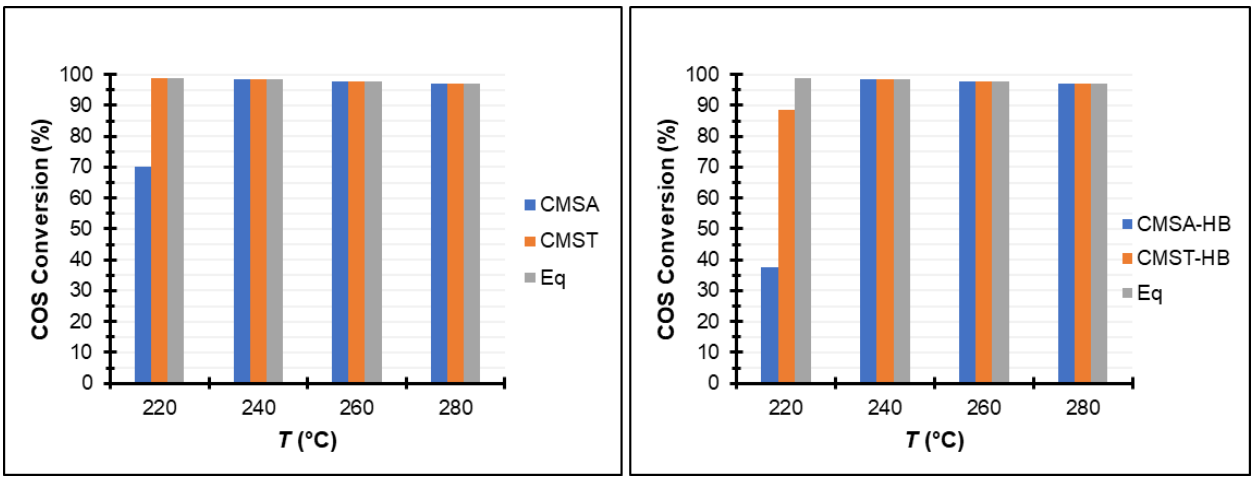

Figure 5. (a) COS conversions offered by CoMo(oxide)/Al_2O_3 (CMSA) or CoMo(oxide)/TiO_2 (CMST) after conventional sulfiding with 2.5 mol% H_2S; and (b) COS conversions offered by CoMo(oxide)/Al_2O_3 (CMSA-HB) or CoMo(oxide)/TiO_2 (CMST-HB) after being exposed to 10% H_2 in balance N_2 at 260 °C for 8 hrs prior to conventional sulfiding with 2.5 mol% H_2S.

3.2.2. H_2 Exposure in the Absence of H_2S After Sulfiding

The effect of hydrogen exposure in the absence of H_2S, 10% H_2 in balance N_2 at 260 °C for 8 hrs, on the sulfided form of the catalysts (CoMo(sulfide)/Al_2O_3 or CoMo(sulfide)/TiO_2) is shown in Figure 6b and again, for the sake of comparison, the COS conversions offered after the conventional sulfiding procedure are presented in Figure 6a. This scenario may occur when a sulfur recovery unit goes into hot standby mode with a slight sub-stoichiometric burn in the thermal reactor. Upon inspection of the data presented in Figure 6, it is clear that this exposure had very little to no impact on catalyst activity. Note that the CoMo(sulfide)/Al_2O_3 COS conversion at 220 °C was in the kinetically limited regime (*i.e.*, conversion was occurring across the entire length of the bed). Therefore, no loss in conversion at this temperature after the H_2 exposure conditions described indicates preservation of all original catalyst active sites.

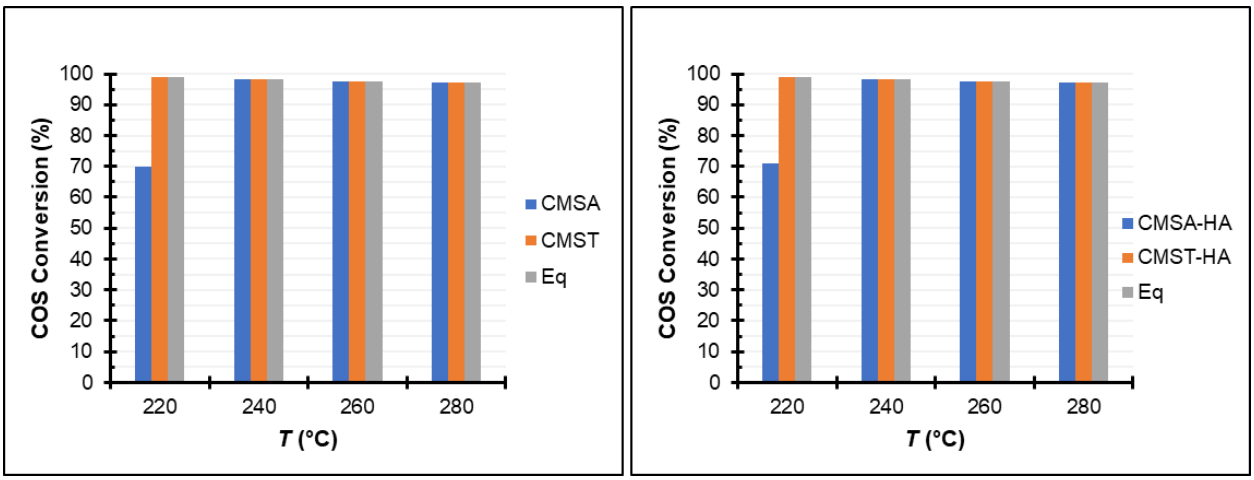

Figure 6. (a) COS conversions offered by CoMo(sulfide)/Al_2O_3 (CMSA) or CoMo(sulfide)/TiO_2 (CMST) after conventional sulfiding with 2.5 mol% H_2S; and (b) COS conversions offered by CoMo(sulfide)/Al_2O_3 (CMSA-HA) or CoMo(sulfide)/TiO_2 (CMST-HA) exposed to 10% H_2 in balance N_2 at 533K for 8 hrs after conventional sulfiding with 2.5 mol% H_2S.

3.2.3. Examining the Impact of H_2 Exposure in the Absence of H_2S on an Alumina-Supported CoMo Catalyst by use of Thermal Gravimetric Analysis

The TGA curves in Figure 7a show the effect of hydrogen exposure in the absence of H_2S before the sulfidation process on an alumina-supported material (CoMo(oxide)/Al_2O_3). It is noted that the CoMo(oxide)/Al_2O_3 sample was pretreated at 323 °C for 3 hrs. Therefore, the weight loss as shown in the red line was attributed to the reduction of Mo and / or Co species. In some instances, the reduced species are more difficult to sulfide and, if the metallic species is generated, the reduction can be irreversible due to slab agglomeration [20, 27]. The grey line in Figure 7a shows the weight gain during the normal sulfiding process, after the H_2 exposure conditions.

The TGA curves in Figure 7b show the effect of hydrogen exposure after the sulfiding process. After exposure to the normal sulfiding conditions, albeit for only 5 hrs (black curve), the hydrogen exposure in the absence of H_2S was initiated. In this case, the ensuing weight loss was predominantly attributed to the removal of the physically adsorbed H_2S and H_2O (red curve). However, it appeared the weight loss was fully recovered when the H_2S was reintroduced to the system (grey curve).

Note that while the H_2 exposure experiments conducted in the catalytic reactor system to probe the resulting impact on activity were performed at 260 °C, these analogous TGA experiments were executed at 323 °C.

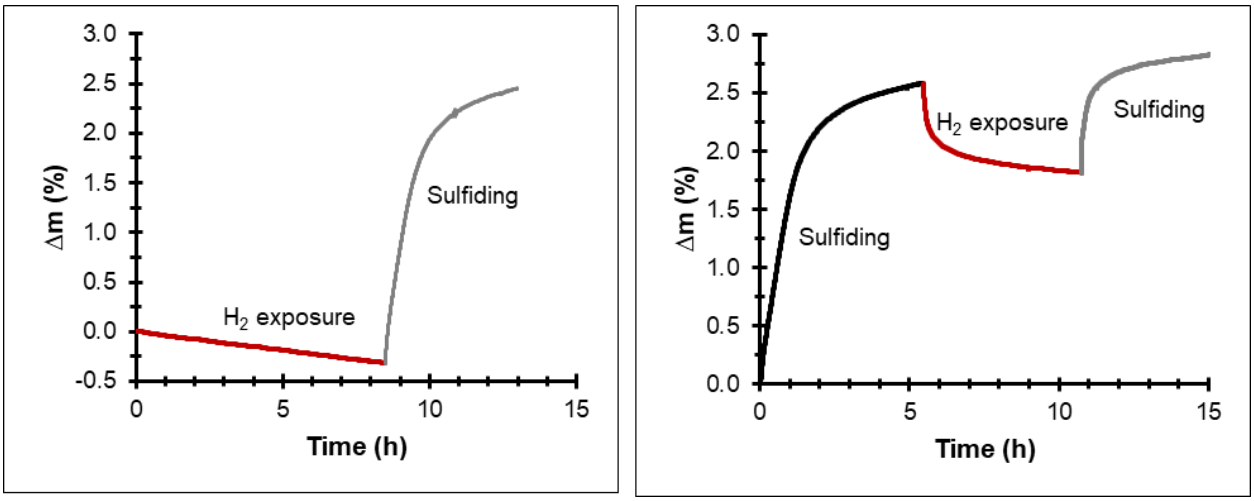

Figure 7. (a) TGA curves of CoMo(oxide)/Al_2O_3 treated with H_2 (10 mol% H_2 in He for 8 hrs, red line) followed by normal sulfidation (2.5 mol% H_2S and 10 mol% H_2 in helium, grey line) and (b) TGA curves of CoMo(oxide)/Al_2O_3 treated with normal sulfidation (black line), the exposure of H_2 (10 mol% H_2 in He, red line), and then normal sulfiding conditions (grey line). In (a) and (b), T = 323.40 ±0.03 °C.

3.3. Effect of O_2 ingress

When in-line burners are used for reheating a tail gas, they are operated substoichimetrically to avoid any O_2 slip and subsequent ingress into the hydrogenation reactor. However, this has to be balanced with the potential for soot formation if the flame is too lean in O_2. In some cases, sometimes outside of operator control, O_2 does end up entering the hydrogenation reactor. The effect of 0.5 mol% O_2 ingress on conventionally sulfided CoMo(sulfide)/Al_2O_3 and CoMo(sulfide)/TiO_2 are presented in Figures 8 and 9. For reference, the baseline performance for CoMo(sulfide)/Al_2O_3 and CoMo(sulfide)/TiO_2 after conventional sulfiding, with no O_2 exposure, is also included in these figures.

For both CoMo(sulfide)/Al_2O_3 and CoMo(sulfide)/TiO_2, after 8 hrs of flowing 0.5 mol% O_2 along with the tail gas feed at 553 K, the O_2 was removed from the feed and COS conversion was measured from 493 to 553 K (Figure 8b). While the CoMo(sulfide)/TiO_2 material lost some COS conversion at 280 °C in the presence of 0.5 mol% O_2, equilibrium was quickly restored after removing O_2 from the feed. Compared to the baseline performance (Figure 8a), there was some lingering effect from the O_2 ingress on the conversion at 220 °C where we saw a *ca.* 3% drop below equilibrium (Figure 8b). The CoMo(sulfide)/Al_2O_3 catalyst appeared more sensitive to the O_2 ingress conditions, where a drop in conversion compared to the baseline performance was observed across all experimental test temperatures. Note an actual net production of COS was measured at 220 and 240 °C. This net production can be attributed to the competing sour gas shift reaction referenced above.

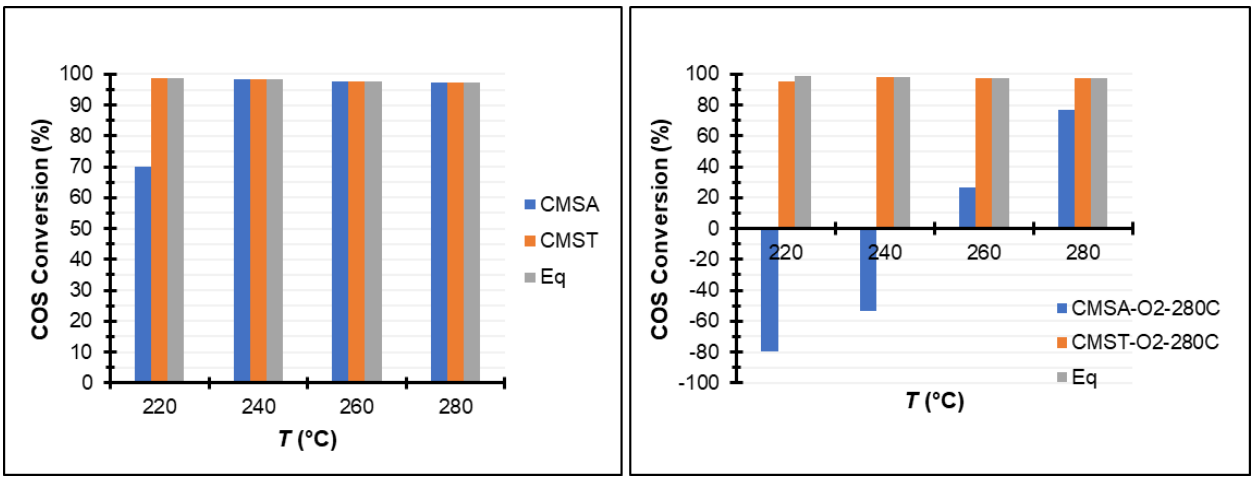

Figure 8. (a) COS conversions offered by CoMo(sulfide)/Al_2O_3 (CMSA) and CoMo(sulfide)/TiO_2 (CMST) after conventional sulfiding with 2.5 mol% H_2S; and (b) COS conversions offered by CoMo(sulfide)/Al_2O_3 (CMSA-O2-280C) and CoMo(sulfide)/TiO_2 (CMST-O2-280C) after being exposed to 0.5% O_2 in the tail gas feed at 280 °C for 8 hrs after conventional sulfiding with 2.5 mol% H_2S.

Similar to above, both CoMo(sulfide)/Al_2O_3 and CoMo(sulfide)/TiO_2 were exposed to 0.5 mol% O_2 along with the normal tail gas feed but a temperature excursion to 400 °C was simulated. Interestingly, compared to the 260 °C exposure test, the O_2 ingress at 400 °C was less damaging to the CoMo(sulfide)/Al_2O_3 material but more detrimental to the CoMo(sulfide)/TiO_2 catalyst. After the exposure conditions, a deviation away from equilibrium was observed for CoMo(sulfide)/TiO_2 for $T \leq 260$ °C (Figure 9b). This time, the loss in conversion for CoMo(sulfide)/Al_2O_3 was more comparable to CoMo(sulfide)/TiO_2, with only a small net production of COS at 200 °C (Figure 9b).

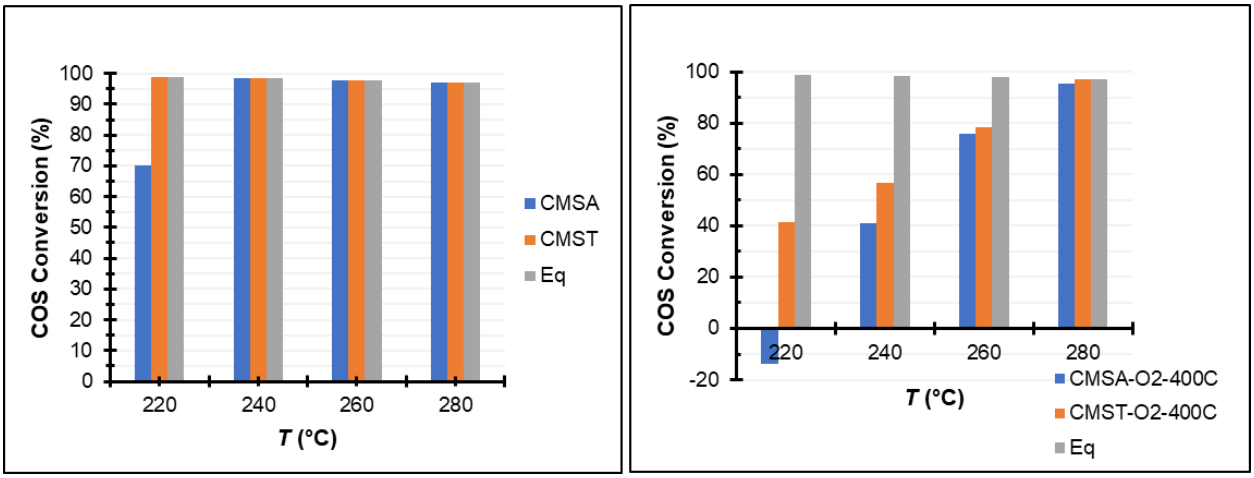

Figure 9. (a) COS conversions offered by CoMo(sulfide)/Al_2O_3 (CMSA) and CoMo(sulfide)/TiO_2 (CMST) after conventional sulfiding with 2.5 mol% H_2S; and (b) COS conversions offered by CoMo(sulfide)/Al_2O_3 (CMSA-O2-400C) and CoMo(sulfide)/TiO_2 (CMST-O2-400C) to 0.5% O_2 in the tail gas feed at 400 °C for 8 hrs after conventional sulfiding with 2.5 mol% H_2S.

To try to gain a better understanding of the catalytic behavior of these two materials, they were characterized by N_2 physisorption, PXRD, TEM, and XPS.

3.4. N_2 Physisorption

All N_2 physisorption results are presented in Figure 10 (*a* and *c*) exhibited Type IV isotherms, indicating that all the catalyst materials tested here were mesoporous [28]. Note that this method does not offer microporous distributions. In the high relative pressure range of 0.6–0.98 $p/p°$, all curves showed H2 hysteresis loops [29], suggesting that the pores were made up by the void space between aggregated particles [30]. The Barrett-Joyner-Halenda adsorption pore size distributions of these materials are also shown in Figure 10 (b and d). A peak shift was observed after the deposition of the Co-Mo oxides on the γ-Al_2O_3 (*i.e.*, the mesopore peak shifted from 10.5 to 9.6 nm, Figure 10b). However, the pore size peak maintained the same position after the sulfiding and catalytic testing, even though the pore volume dropped (Figure 10b). Both the pore size and pore volume reduction were attributed to the calcination effect and the deposition of the Co-Mo species. For the same reasons, the surface areas and total pore volumes of these materials decreased after the deposition, sulfiding, and performance testing (see Table 1). Even though the MoS_2 slabs formed here were too large to be accommodated by the γ-Al_2O_3 mesopores (as will be explained in section 3.6), some cobalt cations may have been able to enter [6].

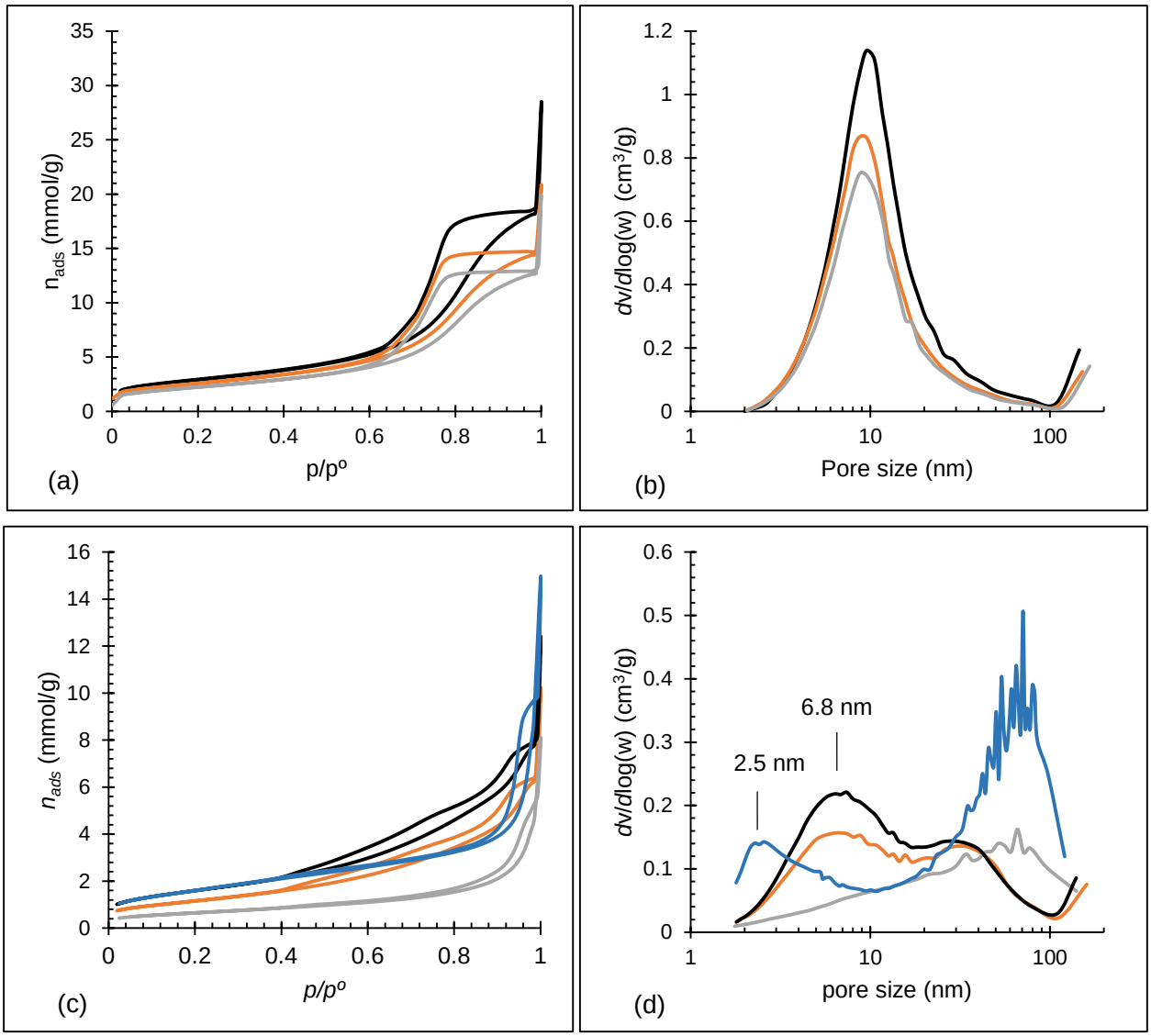

Figure 10. (a) The N_2 isotherms of γ-Al_2O_3 (black), CoMo(oxide)/Al_2O_3 (orange), and CoMo(sulfide)/Al_2O_3 (grey); and (b) The Barrett-Joyner-Halenda adsorption pore size distributions of γ-Al_2O_3 (black), CoMo(oxide)/Al_2O_3 (orange), and CoMo(sulfide)/Al_2O_3 (grey); (c) the N_2 isotherms of the anatase TiO_2 support (blue, before compression), anatase TiO_2 support (black, after compression), CoMo(oxide)/TiO_2 (orange), and CoMo(sulfide)/TiO_2 (grey); and (d) the Barrett-Joyner-Halenda adsorption pore size distributions of anatase TiO_2 (black), CoMo(oxide)/TiO_2 (orange), and CoMo(sulfide)/TiO_2 (grey).

Table 1. N_2 physisorption analysis: summary of the surface area, pore volume, and pore size of fresh and sulfided / used catalysts.

Sample	S_{BET} [a] $m^2\ g^{-1}$	micropore area [b] $m^2\ g^{-1}$	V_{pore} [c] $cm^3\ g^{-1}$	D_{pore} [d] nm
γ-Al_2O_3	230.8 ± 0.7	17.37 ± 0.07	0.83	14
CoMo(oxide)/Al_2O_3	205.4 ± 0.4	12.40 ± 0.06	0.63	12
CoMo(sulfide)/Al_2O_3 [e]	179.3 ± 0.4	11.28 ± 0.05	0.57	13
Anatase TiO_2	130.8 ± 0.4	-	0.45	14
Anatase TiO_2 [f]	129.8 ± 0.3	-	0.36	11
CoMo(oxide)/TiO_2	76.2 ± 0.2	-	0.30	15
CoMo(sulfide)/TiO_2 [e]	51.7 ± 0.1	-	0.22	17

Note: [a]Brunauer-Emmet-Teller surface area; [b]*t*-plot; [c]single point adsorption pore volume; [d] adsorption average pore size; [e]sulfided / used catalysts, and [f]after compression and recalcination.

Figure 10 (*c* and *d*) show that both the isotherms and pore size distributions of the anatase TiO_2 support significantly changed after compression for making pellets, impregnation and deposition of the Co-Mo oxides, and the sulfidation and catalytic processes. The original TiO_2 had two types of pores: (i) the mesopores centered at 2.5 nm are due to the void space between the anatase crystallites with $d = ca.$ 7 nm, and (ii) 30–80 nm pores between the spherical aggregated particles. The bumpy top in the range of 30–80 nm was attributed to the spherical aggregates having a wide range of particle sizes, which caused the void space volume to change. Generally, the void space was larger if the surrounding particles were larger, and vice versa. After compression, the reorganization of the bimodal pore-size distribution was likely due to the dissolving of some TiO_2 nanoparticles (H_2O added to make a paste) and the sintering effect during the compression and recalcination processes. There was not much change after the impregnation process, except for the reduction of the 6.8 nm peak. This 6.8 nm peak was not as pronounced after sulfiding and use in performance tests, potentially due to pore condensation of sulfur that wasn't completely removed before these surface measurements. The surface areas and total pore volumes all decreased after the compression, impregnation, sulfidation and catalytic processes (See Table 1), because of the pore-filling by Co-Mo species and sintering.

3.5. Powder X-Ray Diffraction Patterns

PXRD has been widely used for the characterization of Co-Mo oxides and sulfides. As shown in Figure 11a, the CoMo(oxide)/Al_2O_3 showed peaks belonging to *α*- and *h*-MoO_3. These same peaks were not detected when analyzing the TiO_2-supported material (CoMo(oxide)/TiO_2, Figure 11b). This may be attributed to better dispersion of Co-Mo on the TiO_2 support resulting in a smaller crystallite size. After sulfiding and catalyst testing, the MoO_3 was no longer observed on the alumina-supported material but 2H MoS_2 was detected (CoMo(sulfide)/Al_2O_3, Figure 11a). Again, this same peak was not detected on the sulfided TiO_2 supported material (Figure 11b). Interestingly, after exposing the TiO_2 supported material to H_2 in the absence of H_2S prior to sulfiding, a clear 2H MoS_2 had appeared in the PXRD pattern (Figure 11b). This could be

indicative of an increase in crystallite size which would correspond with poorer dispersion. However, the sharp 2H MoS_2 peak was not observed when the TiO_2-supported material was exposed to the same conditions after sulfiding. The fate of the 2H MoS_2 peak on the alumina supported material was less clear after the H_2 exposure tests before and after sulfiding. Most noticeable when the exposure occurred before sulfiding, the 311 γ-Al_2O_3 and 100 2H MoS_2 peaks broadened and appeared to coalesce (Figure 11a). This may be due to increased interaction of the 2H MoS_2 with this γ-Al_2O_3 face after the H_2 exposure conditions. Where the 2H MoS_2 peak has coalesced with the γ-Al_2O_3 peak, it is difficult to make any inferences regarding crystallite size. While not to the same extent, the 2H MoS_2 on the alumina supported material was also less defined when exposed to H_2 in the absence of H_2S after sulfiding. Where no loss in catalyst activity was observed after this test, this may be attributed to some experimental error when preparing the PXRD sample (*e.g.*, the sample was not ground to the same extent) which resulted in less resolution. It is also possible there was a change in 2D MoS_2 crystallite morphology that did not manifest in reactivity changes.

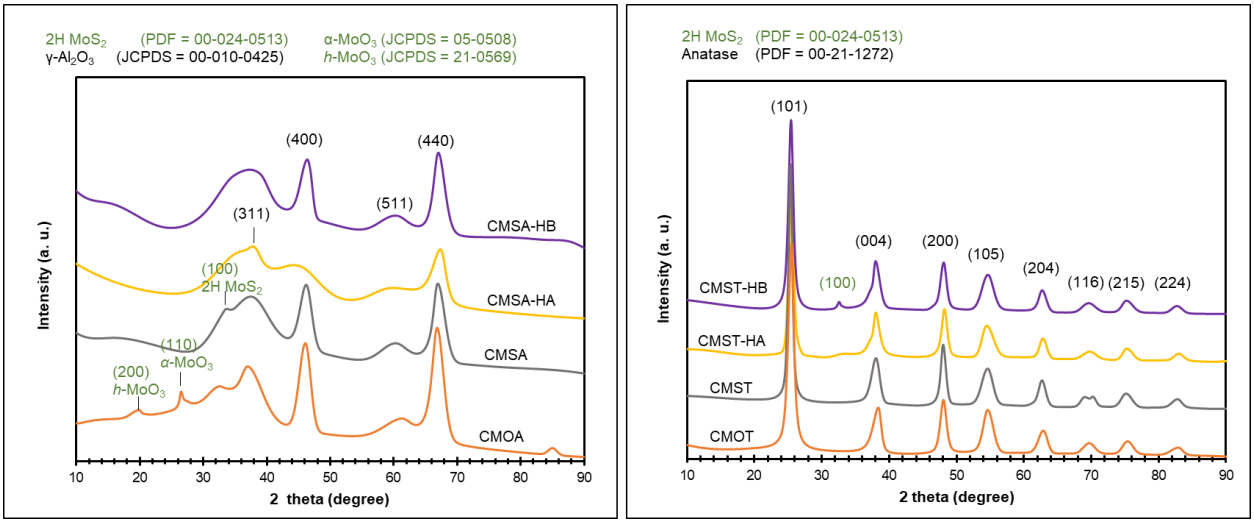

Figure 11. (a) PXRD patterns of CoMo(oxide)/Al_2O_3, CoMo(sulfide)/Al_2O_3, CoMo(oxide)/Al_2O_3 after exposure to H_2, and CoMo(sulfide)/Al_2O_3 after exposure to H_2. Note: the peak indexes in black belong to γ-Al_2O_3, and the indexes in green belong to MoS_2 or MoO_3. (b) PXRD patterns of CoMo(oxide)/TiO_2, CoMo(sulfide)/TiO_2, CoMo(oxide)/TiO_2 after exposure to H_2, and CoMo(sulfide)/TiO_2 after exposure to H_2. Note: the peak indices in black belong to anatase TiO_2, and the index in green belongs to 2H MoS_2.

3.6. High Resolution Transmission Electron Microscopy and Selected Area Electron Diffraction Analyses

HRTEM has also emerged as an important tool for analyzing supported Co-Mo catalysts [19, 31, 32]. After deposition of the Co-Mo precursors and calcination, randomly-oriented MoO_3 needles with a length of *ca.* 50 nm appeared on the γ-Al_2O_3 support (Figure 12a). Based on the N_2 physisorption results, most mesopores in the γ-Al_2O_3 support were in the 10 nm range. Therefore, these MoO_3 needles had to be in macropores or on the surface of the Al_2O_3 pellets. The SAED

analysis revealed nanocrystallites of both α- and *h*-MoO_3 besides the γ-Al_2O_3 background (Figure 12b), in line with the PXRD results. In the sulfided sample (CoMo(sulfide)/Al_2O_3), while the MoO_3 needles disappeared, ubiquitous 2D structures of 2H MoS_2 with a signature spacing between slabs of 0.64 nm were found standing on the surface of the Al_2O_3 support (Figures 12c and 12d), also supporting the PXRD results (Figure 11a). The length of MoS_2 slabs was less than 10 nm (Figure 12d).

Compared to the Al_2O_3-supported Co-Mo catalyst, the TiO_2-supported counterpart showed different results (Figure 13). Instead of MoO_3 needles, as was observed for Al_2O_3, MoO_3 slabs were formed on CoMo(oxide)/TiO_2 (Figure 13 a). We also saw α- and γ-MoO_3 crystallites on the CoMo(oxide)/TiO_2 sample that were identified by their signature d-spacing (not to be confused with space between slabs); 0.39 and 0.59 nm for α-MoO_3 and 0.25 nm for γ-MoO_3 (Figure 13b). Different approaches have been reported for synthesizing MoO_3 slabs in the literature [33-35]. It is noted that the MoO_3 nanocrystallites (*ca*. 5-10 nm) in TiO_2 were smaller than those in Al_2O_3 (*ca*. 50 nm). We contend that the 30-80 nm pores of the TiO_2 support could host the majority of the MoO_3 particles and slabs, leading to better distribution. For the sulfided sample (CoMo(sulfide)/TiO_2), the SAED technique was not sensitive enough to detect crystalline Mo phases and only showed the anatase TiO_2 in the support (Figure 13c). Thus, HRTEM was required to see crystalline Mo species (Figure 13d). Comparing Figures 12d and 13d, it appears there were fewer standing 2H MoS_2 slabs formed on TiO_2 compared to Al_2O_3. However, this may also just be a consequence of better dispersion leading to smaller slabs that are difficult to see. Lastly, a 1T MoS_2 crystalline phase (d spacing of 0.38 nm) was observed on TiO_2 but not on Al_2O_3 (Figure 12d versus 13d). While 2H MoS_2 has been overwhelmingly studied in this application, very few investigations have been reported on the activity of 1T MoS_2 [36].

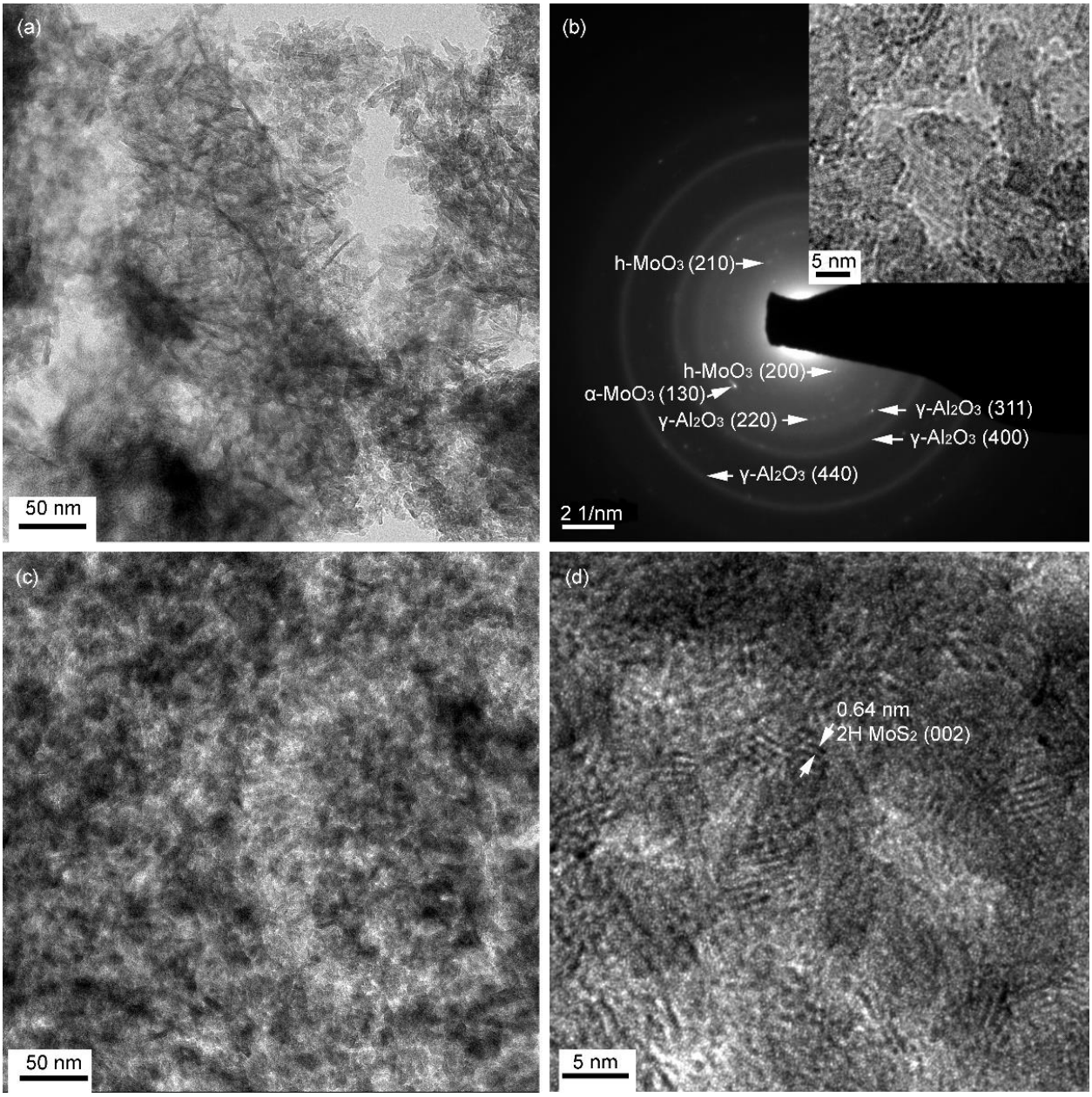

Figure 12. (a) TEM and (b) SAED images of CoMo(oxide)/Al_2O_3; (c) TEM and (d) HRTEM images of CoMo(sulfide)/Al_2O_3.

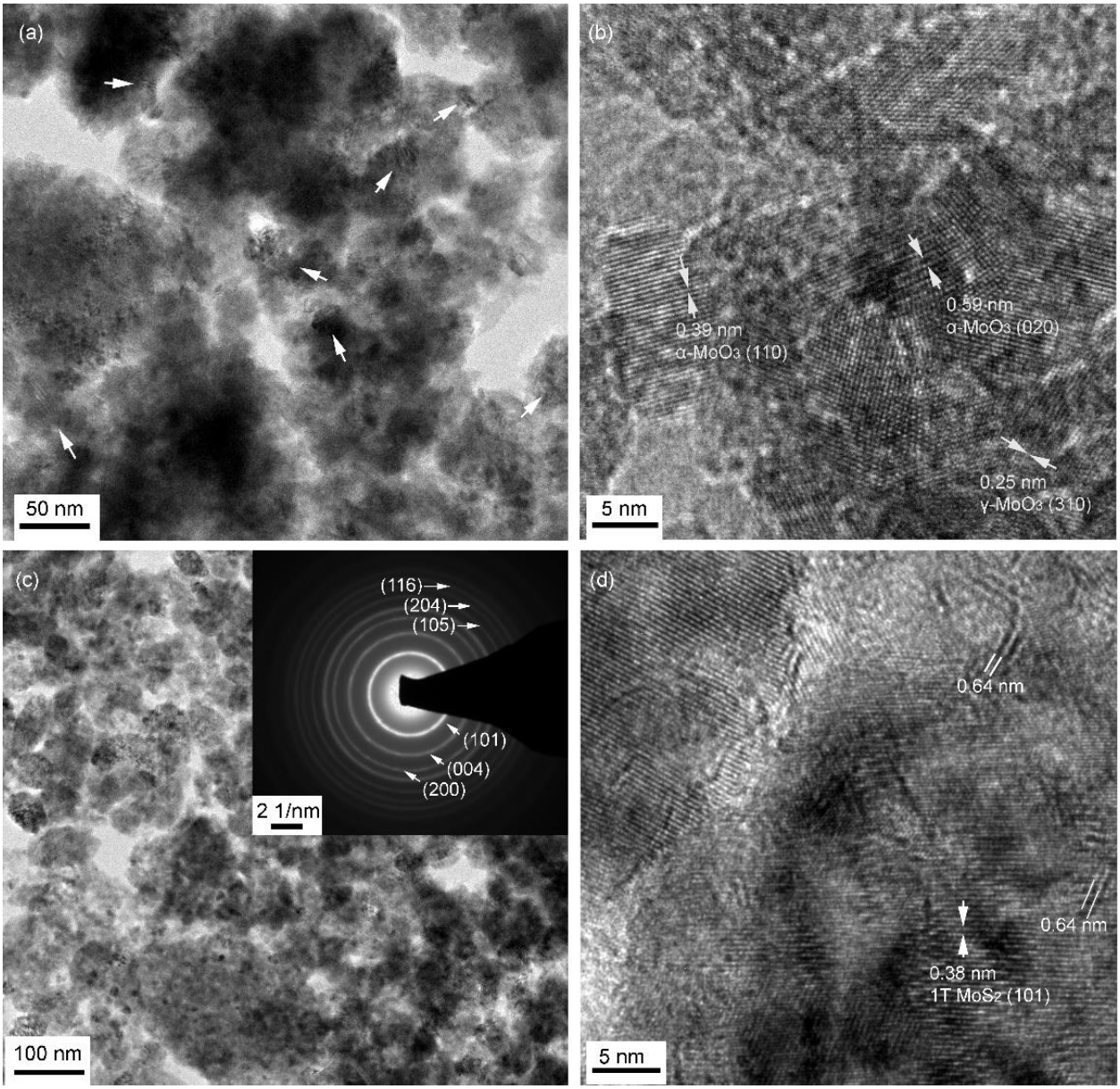

Figure 13. (a) TEM and (b) HRTEM images of CoMo(oxide)/TiO_2; (c) TEM and SAED (inset), and (d) HRTEM images of CoMo(sulfide)/TiO_2.

Figure 14 shows the effect of H_2 exposure, before and after sulfiding, on the morphology of the catalysts. When the CoMo(oxide)/TiO_2 was exposed to hydrogen in the absence of H_2S before sulfidation, the distance between the MoS_2 slabs increased from 0.6-0.7 nm to 0.7-0.9 nm. Is likely due to crystallite coalescence (scintering). As described in the next XPS section, there was a transformation of $Co(OH)_2$ into Co_9S_8 after the normal sulfiding and performance testing. If this transformation occurred between the resulting 2D MoS_2, it may cause the increased interspacing. Interestingly, exposure of the CoMo(sulfide)/TiO_2 material to hydrogen appeared to result in more metastable 1T MoS_2. Figure 14b shows the FFT image of the 1T MoS_2 nanocrystalline phase. The 1T phase has been reported to convert to 2H MoS_2 at 368 K [37]. The high thermal stability of the

1T crystalline phase in our case was possibly due to the intercalated Co compounds that interacted with the 1T MoS_2 sheets. Additionally, no increase in spacing between the 2H MoS_2 slabs was found when the TiO_2 supported material was exposed to H_2 after sulfiding. Similarly, the 2H MoS_2 slab spacing expansion was also found in the CoMo(oxide)/TiO_2 catalyst exposed to H_2 (Figure 14c) but not the CoMo(sulfide)/TiO_2 catalyst exposed to H_2 (Figure 14d).

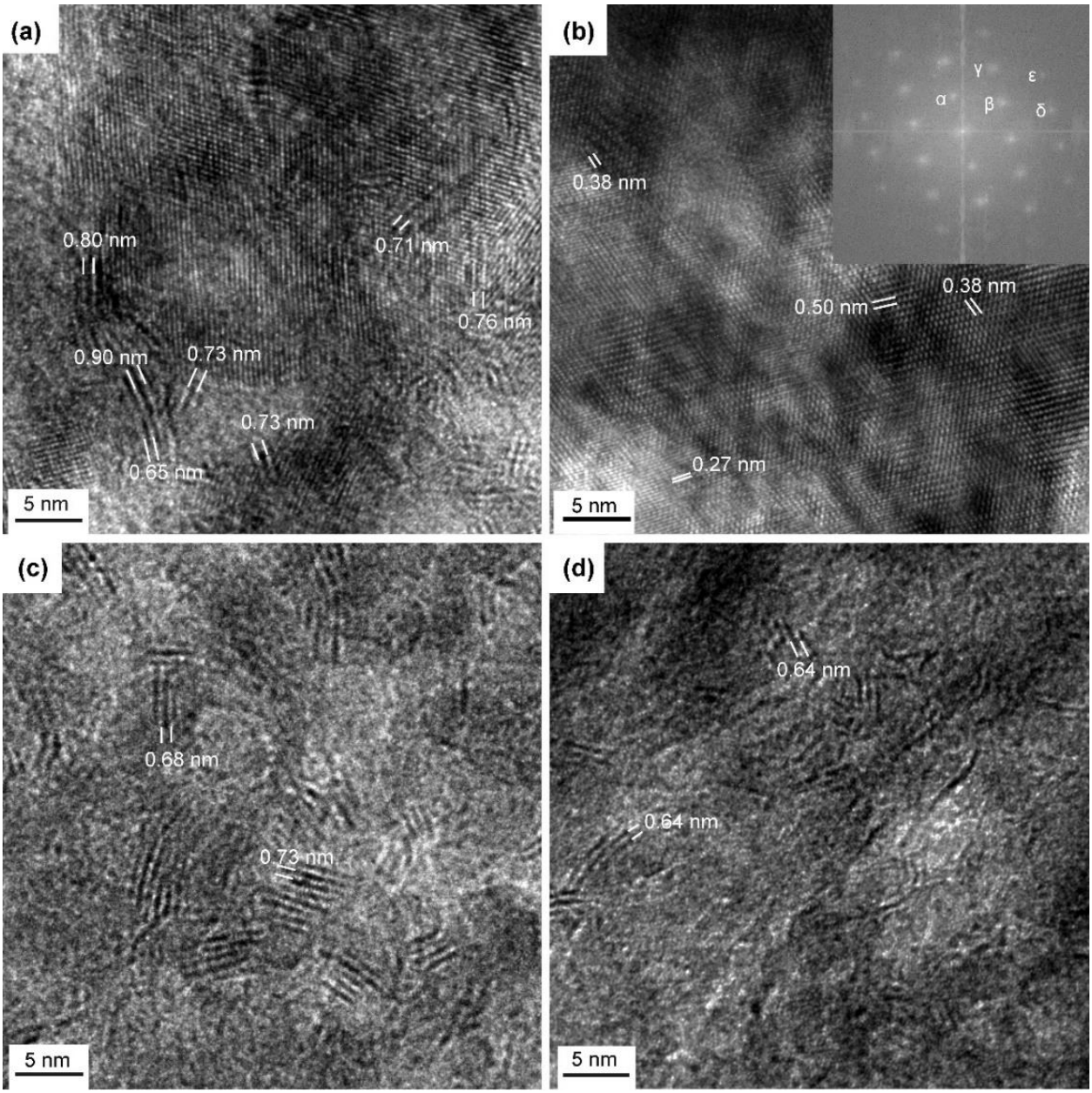

Figure 14. The HRTEM image of CoMo(oxide)/TiO_2 catalyst exposed to H_2, CoMo(sulfide)/TiO_2 catalyst exposed to H_2 (b) with FFT calculation (inset, the d-spacings are listed in Table 2), CoMo(oxide)/Al_2O_3 catalyst exposed to H_2 (c), and CoMo(sulfide)/Al_2O_3 catalyst exposed to H_2 (d).

Table 2. Crystalline plane assignment of FFT results from HRTEM of the 1T MoS_2 on CoMo(sulfide)/TiO_2.

FFT dots	α	β	γ	δ	E	ζ	η
d-spacing (nm)	0.49	0.38	0.28	0.20	0.19	0.18	0.14
assignment [a]	(100)	(101)	(110)	(112)	(202)	(210)	(220)

Notes: [a] Assignments were based on literature data [37].

Note that the above discussion should be taken in the context that HRTEM examines a very small portion of the catalyst surface area. However, the general comments are based on trends observed in multiple HRTEM images, not just those included here.

3.7. XPS Analysis

Surface hydroxyl groups on the catalyst support are reportedly important as they lead to formation of metal-oxygen-metal bonds (*i.e.*, oxo bonds) with the deposited Co-Mo species, thus helping with distribution [6]. Our XPS characterizations showed the presence of significant surface –OH on both the γ-Al_2O_3 and anatase TiO_2 supports (Figures 15a and 16a). Note the AlO_x/OH, TiO_x/OH, and MoO_x/OH peaks in Figures 15a and a´ and Figures 16a and a´ correspond to lattice oxygen (*i.e.*, bridging hydroxyl groups and oxo bonds). It is noted that after the Co-Mo deposition, there was still surface –OH observed resulting from unreacted surface –OH and formed $Co(OH)_2$ (Figures 15a´, 16a´, 15c, and 16c).

As expected, the sulfiding process caused Mo oxides to form MoS_2 (Figures 15b and b´ / Figures 16b and b´). However, even after the sulfiding process, there were still significant Co-Mo oxides present. Where rigorous efforts were made to avoid oxygen exposure, these oxides were attributed to the bridging oxo bonds between the deposited Co-Mo species and the support. With this said, a higher percentage of the molybdenum was in the form of MoS_2 on the TiO_2-supported catalyst compared to the Al_2O_3 counterpart (65.6% versus 56.0%, respectively). This might be used to explain the higher activity of the CoMo(sulfide)/TiO_2 catalyst. The higher sulfidation rate on CoMo(sulfide)/TiO_2 might be related to the smaller size of MoO_3 as described in the TEM section. It is noted that MoO_3 with a larger size is more difficult for sulfidation. As an extreme situation from the literature, after 4 hrs at a high temperature of 600 °C, only 60.6% of unsupported bulk MoO_3 conversion to MoS_2 was observed with a feed containing 5 wt.% H_2S in H_2 [38]. Based on the XPS results, there was still unsulfided MoO_3, Mo_2O_5, and MoO_2 in the Al_2O_3-supported catalyst. However, in the TiO_2-supported catalysts, there was only unsulfided MoO_3 and Mo_2O_5. The existence of the stable MoO_2 phase contributed to the lower MoS_2 in the CoMo(sulfide)/Al_2O_3 catalyst.

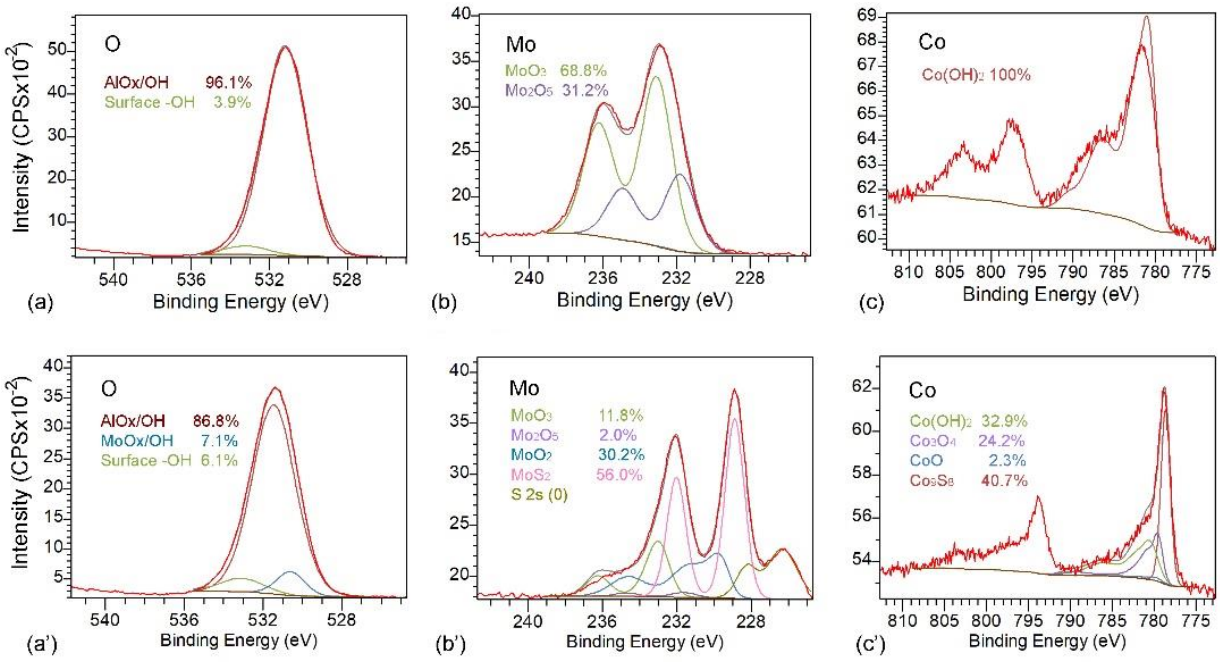

Figure 15. (a) XPS high-resolution scans of oxygen from the samples of Al_2O_3, and (a´) CoMo(oxide)/Al_2O_3; (b) XPS high-resolution scans of molybdenum from the samples of CoMo(oxide)/Al_2O_3, and (b´) CoMo(sulfide)/Al_2O_3; and (c) XPS high-resolution scans of cobalt from the samples of CoMo(oxide)/Al_2O_3, and (c´) CoMo(sulfide)/Al_2O_3 [39]. Notes: The components with the same index are combined for clarity.

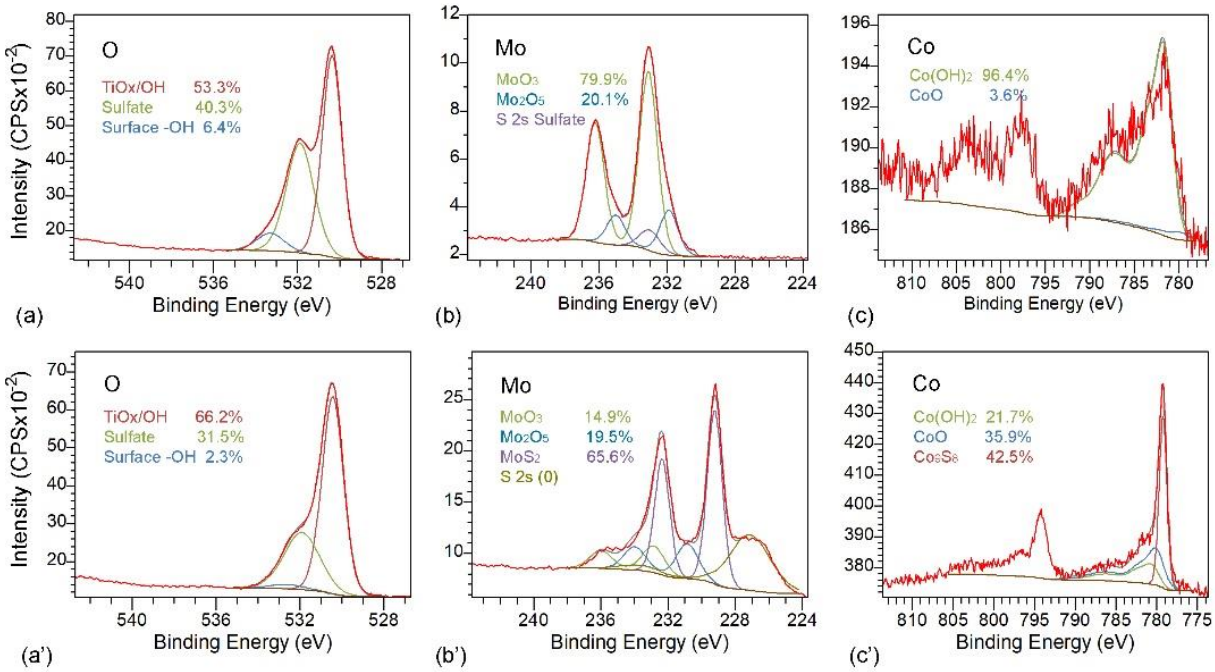

Figure 16. (a) XPS high-resolution scans of oxygen from the samples of TiO_2, and (a´) CoMo(oxide)/TiO_2; (b) XPS high-resolution scans of molybdenum from the samples of CoMo(oxide)/TiO_2, and (b´) CoMo(sulfide)/TiO_2; and (c) XPS high-resolution scans of cobalt from the samples of CoMo(oxide)/TiO_2, and (c´) CoMo(sulfide)/TiO_2 [39]. Notes: The components with the same index are combined for clarity. Notes: The components with the same index are combined for clarity.

In the CoMo(sulfide)/Al_2O_3 and CoMo(sulfide)/TiO_2 materials, *ca.* 40% of cobalt was found in the form of Co_9S_8 that might be active for hydrogenation reactions, but the mechanism is still under debate. While the lower oxidation state of cobalt may be active for hydrogenation, it may also strongly adsorb H_2S which could have a poisoning effect, particularly at lower reaction temperatures. Somewhat surprisingly, there was also 22–33% $Co(OH)_2$. This may be explained by decreased accessibility to the sulfiding conditions by incorporation into the intercalation process between the MoS_2 slabs which was referenced earlier in the HRTEM section [40].

It is worth noting that Ti(III) was observed in both CoMo(oxide)/TiO_2 and CoMo(sulfide)/TiO_2. There was more Ti(III) found in the CoMo(sulfide)/TiO_2 analyses, likely because of the reducing atmosphere during the sulfiding. The existence of Ti(III) is favorable for hydrogenation [13], COS/CS_2 conversion [41], CO oxidation [7], and other reactions [42].

According to Figures 16a and a´, CoMo(sulfide)/TiO_2 had less sulfate than CoMo(oxide)/TiO_2 due to the reduction by H_2/H_2S as seen in the TGA measurements and the excess H_2S observed during sulfiding. As evidenced by the S peaks in Figures 15b´ and 16b´, some residual elemental sulfur (intermediate of the hydrogenation reactions) was still present within the mesopores of the catalysts

4. Conclusions

During sulfiding of tail gas catalysts, it is important to use a sufficiently high H_2S concentration. We observed decreased activity resulting from a catalyst that was sulfided with a 1 mol% H_2S-containing feed when compared to a material that was sulfided with a 2.5 mol% H_2S-containing feed. We believe the lower concentration led to H_2S starvation at the bed outlet early on during the sulfiding procedure. Too high of an H_2S concentration during sulfiding may also have negative repercussions (*e.g.*, an exothermic temperature excursion event that could also damage the catalyst).

A representative tail gas feed was tested for sulfiding Al_2O_3- and TiO_2-supported Co-Mo catalysts at 260 °C and compared to a more conventional sulfiding method that used a 2.5 mol% H_2S, 10% H_2, and balance N_2 feed that included a temperature ramp from 200 to 315 °C. While the conventional method led to more active catalysts in both cases, depending on the conditions, sulfiding with a Claus tail gas itself may lead to sufficient reactivity. When measuring kinetically limited COS conversion over the course of 30 hrs, conversion did not obviously increase with increased time on stream. This would indicate temperature is more important than time when sulfiding tail gas catalysts.

In our lower temperature tests, the TiO_2-supported catalysts offered higher activity than the Al_2O_3-supported counterpart; four reasons were considered for explaining this. First, the 30-80 nm pores of the anatase TiO_2 support were large enough to accommodate MoS_2 crystallites. This led to more edges and defects compared to the larger the MoS_2 crystallites on Al_2O_3 which were presumably located on the exterior surface or within macropores. Secondly, based on XPS analyses, the anatase titania support led to a higher MoS_2 concentration compared to the Al_2O_3-supported material. Thirdly, the Ti(III) found in the titania support was anticipated to be beneficial for the hydrogenation reactions. And lastly, given the higher propensity of TiO_2 for COS hydrolysis, TiO_2-supported materials can better accommodate any loss in the water gas shift reaction that may result in higher COS concentrations.

Based on our performance tests, hydrogen exposure in the absence of H_2S, prior to sulfiding, had a negative impact on the hydrogenation activity of Claus tail gas catalysts. However, the sulfided form of these materials was more robust towards any detrimental effect caused by this exposure condition. From the XRD analyses, it seems the H_2 exposure prior to sulfiding resulted in larger MoS_2 crystallite sizes. From the XPS analyses, it also appeared the H_2 exposure prior to sulfiding resulted in increased spacing between the MoS_2 slabs. At this stage, it is unknown if these two observations are related. Additionally, the effect on catalyst activity caused by increased slab spacing is unknown. However, larger MoS_2 crystallites are presumably less favorable for catalytic performance compared to smaller, better distributed crystallites.

Both the Al_2O_3- and TiO_2-supported catalysts suffered some loss in activity after exposure to oxygen ingress conditions. When the oxygen ingress occurred at 280 °C, the alumina-supported

material was much more sensitive to oxygen ingress. However, when the oxygen ingress was simulated at 400 °C, the losses in activity were more comparable between the two materials.

References

[1] A. PiÉPlu, O. Saur, J.-C. Lavalley, O. Legendre, C. NÉDez, Claus Catalysis and H_2S Selective Oxidation, Catalysis Reviews, 40 (1998) 409-450.

[2] R. Sui, C.B. Lavery, D. Li, C.E. Deering, N. Chou, N.I. Dowling, R.A. Marriott, Improving low-temperature CS_2 conversion for the Claus process by using La(III)-doped nanofibrous TiO_2 xerogel, Applied Catalysis B: Environmental, 241 (2019) 217-226.

[3] W.D. Monnery, W.Y. Svrcek, L.A. Behie, Modelling the modified claus process reaction furnace and the implications on plant design and recovery, The Canadian Journal of Chemical Engineering, 71 (1993) 711-724.

[4] R. Sui, C.B. Lavery, C.E. Deering, R. Prinsloo, D. Li, N. Chou, K.L. Lesage, R.A. Marriott, Improved carbon disulfide conversion: Modification of an alumina Claus catalyst by deposition of transition metal oxides, Applied Catalysis A: General, 604 (2020) 117773.

[5] C. Rhodes, S.A. Riddel, J. West, B.P. Williams, G.J. Hutchings, The low-temperature hydrolysis of carbonyl sulfide and carbon disulfide: a review, Catalysis Today, 59 (2000) 443-464.

[6] H. Topsøe, B.S. Clausen, F.E. Massoth, Hydrotreating Catalysis, in: J.R. Anderson, M. Boudart (Eds.) Catalysis: Science and Technology, Springer Berlin Heidelberg, Berlin, Heidelberg, 1996, pp. 1-269.

[7] M.L. Kazemi, R. Sui, P.D. Clark, R.A. Marriott, Catalytic combustion of Claus tail gas: Oxidation of sulfur species and CO using gold supported on lanthanide-modified TiO_2, Applied Catalysis A: General, 587 (2019) 117256.

[8] R.R. Chianelli, M. Daage, M.J. Ledoux, Fundamental Studies of Transition-Metal Sulfide Catalytic Materials, in: D.D. Eley, H. Pines, W.O. Haag (Eds.) Advances in Catalysis, Academic Press1994, pp. 177-232.

[9] H. Topsøe, The role of Co–Mo–S type structures in hydrotreating catalysts, Applied Catalysis A: General, 322 (2007) 3-8.

[10] S.S. Grønborg, N. Salazar, A. Bruix, J. Rodríguez-Fernández, S.D. Thomsen, B. Hammer, J.V. Lauritsen, Visualizing hydrogen-induced reshaping and edge activation in MoS_2 and Co-promoted MoS_2 catalyst clusters, Nature Communications, 9 (2018) 2211.

[11] N. Salazar, S. Rangarajan, J. Rodríguez-Fernández, M. Mavrikakis, J.V. Lauritsen, Site-dependent reactivity of MoS2 nanoparticles in hydrodesulfurization of thiophene, Nature Communications, 11 (2020) 4369.

[12] E. Payen, J. Grimblot, S. Kasztelan, Study of oxidic and reduced alumina-supported molybdate and heptamolybdate species by in situ laser Raman spectroscopy, The Journal of Physical Chemistry, 91 (1987) 6642-6648.

[13] J. Ramirez, L. Cedeño, G. Busca, The Role of Titania Support in Mo-Based Hydrodesulfurization Catalysts, Journal of Catalysis, 184 (1999) 59-67.

[14] P. Schacht, G. Hernández, L. Cedeño, J.H. Mendoza, S. Ramírez, L. García, J. Ancheyta, Hydrodesulfurization Activity of CoMo Catalysts Supported on Stabilized TiO_2, Energy & Fuels, 17 (2003) 81-86.

[15] S. Dzwigaj, C. Louis, M. Breysse, M. Cattenot, V. Bellière, C. Geantet, M. Vrinat, P. Blanchard, E. Payen, S. Inoue, H. Kudo, Y. Yoshimura, New generation of titanium dioxide support for hydrodesulfurization, Applied Catalysis B: Environmental, 41 (2003) 181-191.
[16] M. Gao, B. Liu, P. Zhao, X. Yi, X. Shen, Y. Xu, Mechanical strengths and thermal properties of titania-doped alumina aerogels and the application as high-temperature thermal insulator, Journal of Sol-Gel Science and Technology, 91 (2019) 514-522.
[17] C. Liu, Z. Zhou, Y. Huang, Z. Cheng, W. Yuan, Support Effects on Thiophene Hydrodesulfurization over Co-Mo-Ni/Al_2O_3 and Co-Mo-Ni/TiO_2-Al_2O_3 Catalysts, Chinese Journal of Chemical Engineering, 22 (2014) 383-391.
[18] P. Afanasiev, Calculation of MoS2 slabs morphology descriptors from transmission electron microscopy data revisited. Case study of the influence of citric acid and treatment conditions on the properties of MoS2/Al2O3, Applied Catalysis A: General, 529 (2017) 10-19.
[19] Y. Li, A. Li, F. Li, D. Liu, Y. Chai, C. Liu, Application of HF etching in a HRTEM study of supported MoS2 catalysts, Journal of Catalysis, 317 (2014) 240-252.
[20] M. Huffmaster, Key to a long and active life - effective activation of low temperature tial gas catalyst and damage avoidance, Brimstone Sulfur SymposiumVail, USA, 2019.
[21] M. Huffmaster, A kinetic model for TGU hydrogenation reactions - what temperature profiles say about catalyst aging and poisoning, Brimstone Sulfur SymposiumVail, USA, 2022.
[22] Y. Okamoto, H. Tomioka, T. Imanaka, S. Teranishi, Surface structure and catalytic activity of sulfided $MoO_3Al_2O_3$ catalysts: Hydrodesulfurization and hydrogenation activities, Journal of Catalysis, 66 (1980) 93-100.
[23] B. Hereijgers, P. van Nisselrooij, B. van de Giessen, M. van Hoeke, The benefit of using titania in Claus and tail gas catalysis, Sulphur, IPCO, 2017.
[24] E. Santacesaria, M. Tonello, G. Storti, R.C. Pace, S. Carrà, Kinetics of titanium dioxide precipitation by thermal hydrolysis, Journal of Colloid and Interface Science, 111 (1986) 44-53.
[25] R. Sui, J.H. Jacobs, N. Chou, C.E. Deering, C.B. Lavery, R.A. Marriott, Facile synthesis of thermally stable anatase titania with a high-surface area and tailored pore sizes, Journal of Sol-Gel Science and Technology, (2023).
[26] P.D. Clark, N.I. Dowling, M. Huang, O. Okemona, G.D. Butlin, R. Hou, W.S. Kijlstra, Studies on sulfate formation during the conversion of H2S and SO2 to sulfur over activated alumina, Applied Catalysis A: General, 235 (2002) 61-69.
[27] K.S. Seshadri, F.E. Massoth, L. Petrakis, Electron spin resonance and microbalance study of sulfided molybdena-alumina catalysts, Journal of Catalysis, 19 (1970) 95-100.
[28] R. Haul, S. J. Gregg, K. S. W. Sing: Adsorption, Surface Area and Porosity. 2. Auflage, Academic Press, London 1982. 303 Seiten, Preis: $ 49.50, Berichte der Bunsengesellschaft für physikalische Chemie, 86 (1982) 957-957.
[29] K.S.W. Sing, R.T. Williams, Physisorption Hysteresis Loops and the Characterization of Nanoporous Materials, Adsorption Science & Technology, 22 (2004) 773-782.
[30] P. Klobes, R. Munro, Porosity and Specific Surface Area Measurements for Solid Materials, Special Publication (NIST SP), National Institute of Standards and Technology, Gaithersburg, MD, 2006.
[31] F. Delannay, High resolution electron microscopy of hydrodesulfurization catalysts: A review, Applied Catalysis, 16 (1985) 135-152.
[32] X. Xi, F. Zeng, H. Cao, C. Cannilla, T. Bisswanger, S. de Graaf, Y. Pei, F. Frusteri, C. Stampfer, R. Palkovits, H.J. Heeres, Enhanced C3+ alcohol synthesis from syngas using

KCoMoSx catalysts: effect of the Co-Mo ratio on catalyst performance, Applied Catalysis B: Environmental, 272 (2020) 118950.
[33] X. Hou, J. Huang, M. Liu, X. Li, Z. Hu, Z. Feng, M. Zhang, J. Luo, Single-Crystal MoO3 Micrometer and Millimeter Belts Prepared from Discarded Molybdenum Disilicide Heating Elements, Scientific Reports, 8 (2018) 16771.
[34] I.A. de Castro, R.S. Datta, J.Z. Ou, A. Castellanos-Gomez, S. Sriram, T. Daeneke, K. Kalantar-zadeh, Molybdenum Oxides – From Fundamentals to Functionality, Advanced Materials, 29 (2017) 1701619.
[35] P.P. Crevier, E. Roisin, G.J. Bloemendal, TG 107 low temperature tail gas treating catalyst is hot stuff, Laurance Reid Gas Conditioning ConferenceNorman, Oklahoma, 2009.
[36] H. Cao, Z. Bai, Y. Li, Z. Xiao, X. Zhang, G. Li, Solvothermal Synthesis of Defect-Rich Mixed 1T-2H MoS2 Nanoflowers for Enhanced Hydrodesulfurization, ACS Sustainable Chemistry & Engineering, 8 (2020) 7343-7352.
[37] F. Wypych, R. Schöllhorn, 1T-MoS_2, a new metallic modification of molybdenum disulfide, Journal of the Chemical Society, Chemical Communications, (1992) 1386-1388.
[38] H. Farag, Effect of Sulfidation Temperatures on the Bulk Structures of Various Molybdenum Precursors, Energy & Fuels, 16 (2002) 944-950.
[39] I. Alstrup, I. Chorkendorff, R. Candia, B.S. Clausen, H. Topsøe, A combined X-Ray photoelectron and Mössbauer emission spectroscopy study of the state of cobalt in sulfided, supported, and unsupported Co□Mo catalysts, Journal of Catalysis, 77 (1982) 397-409.
[40] B.C. Gates, J.R. Katzer, J.H. Olson, H. Kwart, A.B. Stiles, Kinetics and mechanism of desulfurization and denitrogenation of coal-derived liquids. Ninth quarterly report, June 21, 1977--September 20, 1977, United States, 1978.
[41] P.D. Clark, N.I. Dowling, M. Huang, Role of Ti^{3+} in CS_2 conversion over TiO_2 Claus catalyst, Applied Catalysis A: General, 489 (2015) 111-116.
[42] M. Xing, W. Fang, M. Nasir, Y. Ma, J. Zhang, M. Anpo, Self-doped Ti^{3+}-enhanced TiO_2 nanoparticles with a high-performance photocatalysis, Journal of Catalysis, 297 (2013) 236-243.